Revised Manuscript with changes accepted

Published to Marine Ecology Progress Series
Vol. 580: 83–100, 2017
https://doi.org/10.3354/meps12310

Relationship between light, community composition, and the electron requirement for carbon fixation in natural phytoplankton

Yuanli Zhu [1,*], Joji Ishizaka [1], Sarat Chandra Tripathy [2], Shengqiang Wang [3], Chiho Sukigara [4], Joaquim Goes [5], Takeshi Matsuno [6], David J. Suggett [7]

[1] Institute for Space-Earth Environmental Research, Nagoya University, Nagoya 464-8601, Japan

[2] ESSO-National Centre for Antarctic and Ocean Research, Ministry of Earth Sciences, Vasco-da-Gama, Goa 403804, India

[3] School of Marine Sciences, Nanjing University of Information Science and Technology, Nanjing, 210044, Jiangsu, China

[4] Graduate School of Environmental Studies, Nagoya University, Nagoya 464-8601, Japan

[5] Lamont-Doherty Earth Observatory at Columbia University, Palisades, New York 10964, USA

[6]Research Institute for Applied Mechanics, Kyushu University, Fukuoka 812-8581, Japan

[7]Climate Change Cluster, University of Technology Sydney, P.O.Box 123, Broadway, NSW 2007, Australia

Abstract

Fast Repetition Rate fluorometry (FRRf) provides a means to examine primary productivity at high resolution across broad scales, but must be coupled with independent knowledge of the electron requirement for carbon uptake (K_C) to convert FRRf-measured electron transfer rate (ETR) to an inorganic carbon (C) uptake rate. Previous studies have demonstrated that variability of K_C can be explained by key environmental factors (e.g. light, nutrients, temperature). However, how such reconciliation of K_C reflects changes of phytoplankton physiological status versus that of community composition has not been well resolved. Therefore, using a dataset of coupled FRRf and C uptake measurements, we examined how the environmental dependency of K_C potentially varied with parallel changes in phytoplankton community structure. Data was combined from 14 campaigns conducted during the summer season throughout 2007 to 2014 in the East China Sea (ECS) and Tsushima Strait (TS). We demonstrated that K_C varied considerably, but that this variability was best explained by a linear relationship with light availability (R^2 = 0.66). Co-variability between K_C and light availability was slightly improved by considering data as two clusters of physico-chemical conditions (R^2 = 0.74), but was best improved as two taxonomic clusters: samples dominated by micro-phytoplankton (>20 μm) versus small phytoplankton (nano + pico, <20 μm) (R^2 = 0.70-0.81). Interaction of phytoplankton community structure with light availability therefore explains the majority of variance of K_C. The algorithms generated through our analysis therefore provide a means to examine C-uptake with high resolution from future FRRf observations from these waters.

Keywords: ETR Primary productivity Quantum requirement for carbon fixation Phytoplankton composition Fast repetitive rate fluorometer

INTRODUCTION

Fast Repetition Rate fluorometry (FRRf, Kolber et al. 1998) has been widely considered a key progress for aquatic research in global efforts to better understand environmental regulation of primary productivity (Suggett et al. 2009b). A substantial number of studies have now demonstrated co-variance between parallel measurements of FRRf derived electron transport rates (ETRs) and C-uptake rates (e.g. Suggett et al. 2009a and references therein; Cheah et al. 2011, Robinson et al. 2014, Schuback et al. 2015), providing strong evidence that FRR fluorometers could potenitally examine patterns of carbon uptake through application of an "electron requirement for C-fixation" conversion factor (Lawrenz et al. 2013, Hancke et al. 2015; termed K_C). However, past parallel measurements of ETRs and C-uptake rates in fact show that K_C is highly variable since numerous factors can cause cellular processes to consume ETR-derived energy and reductant that is otherwise used for C assimilation (e.g. Lawrenz et al. 2013, Halsey & Jones 2015); consequently, use of an assumed constant for K_C is a likely cause for many FRRf based overestimates of productivity rates (Kromkamp et al. 2008; Mino et al. 2014), in particular under excess irradiance (Ralph et al. 2010).

Recent research has investigated and modeled K_C variability in an attempt to better constrain FRRf-based estimates of phytoplankton carbon fixation. Lawrenz et al. (2013) synthesized global FRRf-based K_C data and demonstrated that this parameter could often be predicted as a function of key environmental factors that regulate phytoplankton productivity and community structure, notably light, temperature and inorganic nutrient availability. However, the specific relationship between these factors and K_C differed between oceanic regions of interest. More recently, Schuback et al. (2015, 2016) further demonstrated that K_C variance throughout iron limited waters could be explained by co-variance with the extent of non-photochemical quenching status (NPQ), interpreted

as an indication of processes consuming photosynthetically derived energy and hence decoupling linear electron flow from carbon uptake. Whilst environmental regulation of K_C variability is clearly apparent, other studies note that changes in phytoplankton community structure may contribute to this variance (see Suggett et al. 2006a, 2009a, Robinson et al. 2014). Such an observation is perhaps unsurprising where both ETR (e.g. Cermeño et al. 2005, Giannini & Ciotti 2016) and carbon uptake rate (e.g. Tripathy et al. 2014, Barnes et al. 2015) vary across phytoplankton taxa, often as a first order function of cell size, as a result of changes in prevailing hydrographic condition. Variability of K_C across phytoplankton species has been examined for few laboratory cultures (Suggett et al. 2009a, Brading et al. 2013, Hoppe et al. 2015), and the potential influence of phytoplankton composition on K_C for natural field samples remains largely unexplored (Suggett et al. 2006a, Robinson et al. 2014).

To examine for the potential influence of phytoplankton community composition upon K_C variability, we analyzed data from 14 experiments from 9 cruises conducted in the East China Sea (ECS) and Tsushima Strait (TS) over a period of 8 years (2007 to 2014). The entire ECS and TS region is a very productive and highly dynamic region because of the seasonal fluctuation of several different water masses (Fig. 1). In summer, waters are characterized by high nutrient concentrations and elevated phytoplankton biomass (Chl-a) in western regions as a result of the discharge from Changjiang River (i.e. Changjiang Diluted Water, CDW), which constitutes about 85% of the total discharge by all rivers into ECS (Ning et al. 1998). A pattern of depleted nutrients in parallel with low Chl-a is generally observed for the upper layer of eastern ECS (Gong et al. 2003). Water mass for TS mainly originates from ECS in summer (Guo et al. 2006) and is partly formed by the Kuroshio water, which flows northeastward along the eastern margin of the ECS continental shelf. Whilst CDW can potentially extend into TS, nutrients are likely depleted before reaching TS

(Morimoto et al. 2009). As such, the bio-optical properties as well as phytoplankton size structure appear notably different between TS and ECS (Wang et al. 2014), providing an ideal study region to examine variability in K_C.

We recently reported strong, but non-linear, correlation between parallel measures of FRRf-based ETRs and C-uptake rates for a semi-enclosed bay (Ariake Bay). Variance of K_C derived from these parallel measures appears largely explained by light availability (Zhu et al. 2016). However, phytoplankton community composition remained generally unchanged throughout the Ariake Bay dataset, and as yet it is unclear whether this light-dependent regulation of K_C is potentially further influenced by the dominant phytoplankton species present. To test for this potential influence, we therefore specifically examined parallel FRRf measurements and 24h on-deck ^{13}C incubation from the ECS and TS that were collected under diverse prevailing environmental conditions (e.g. light, nutrients) as well as phytoplankton community structure. We specifically (i) tested whether light dependent variability of K_C (derived from 24h on deck ^{13}C uptake) observed for Ariake Bay was similarly observed across the broader biogeographic domain of the ECS and TS; and (ii) evaluated the extent to which the phytoplankton community structure, as determined from high performance liquid chromatography (HPLC), further influenced the environmental dependency of K_C. Together we used these data to further develop a specific K_C algorithm for this region and hence a practical FRRf based method for more broadly examining carbon uptake dynamics in the ECS and TS.

MATERIALS AND METHODS

Sampling area, sites and dataset

Analyzed datasets were from 14 (12 for parallel measured ^{13}C-ETR) campaigns conducted across the ECS and TS region (Fig. 1) during the summers of 2007-2014 (Table 1). Water mass interactions in this region are complex and in summer influenced by CDW from the east, the Taiwan Warm Current (TWC) from the south, the Kuroshio branch water (KBW) from the west and the Yellow Sea Cold Water (YSCW) from the north (Fig. 1). Stations for conducting parallel FRRf and C-uptake rate measurements were located in three sub-areas of this region: the mid-shelf of ECS, outer-shelf of ECS and the TS (Fig. 1, Table 1).

Sampling and measurements of physical and biochemical properties

Sampling protocols for all parameters and ^{13}C experiments employed in our study are similar to those reported previously (Siswanto et al. 2006, Wang et al. 2014, 2015; see also Zhu et al. 2016 for Ariake Bay). Seawater samples for ^{13}C-uptake experiments for all cruises were collected before sunrise, from six depths corresponding to light levels of approximately 100, 50, 25, 10, 5 and 1% of the surface Photosynthetically Active Radiation (PAR, 400 - 700 nm). Water was sampled using a rosette equipped with twelve × 5L Niskin bottles (General Oceanics, USA) and a conductivity-temperature-depth profiler (CTD, 911+, SeaBird Electronics, USA). Sampling depths were determined by a high-resolution profiling reflectance radiometer (PRR-800/810, Biospherical Instruments, USA) profile conducted one day prior to incubations. Incident PAR at the sea surface (E_0^+) was measured throughout the sample incubating period with a quantum scalar irradiance sensor (QSL-2100, Biospherical Inc., USA) mounted on the incubators. *In situ* underwater

irradiance field $E_d^-(\lambda, z)$ was measured during the incubation period for 13 wavelengths (λ = 380, 412, 443, 465, 490, 510, 532, 555, 565, 589, 625, 665 and 683 nm) using the PRR-800 profiled every 2 hours from 10:00-16:00 (local time), from the surface to euphotic depth (Z_{eu}, defined as the depth with 1% of surface PAR). Repeated profiles were conducted every two hours, according to a Lagrangian approach via a buoy track to enable repeat measurements on the same water mass.

Seawater samples were processed as follows for Chl-a, nutrients and phytoplankton light absorption measurements. An aliquot of 100 mL seawater was filtered onto 25 mm glass fiber filters (Whatman GF/F) under low vacuum pressure (<0.02 MPa) to determine Chl-a content. Filters were extracted in N, N-dimethylformamide for 24h in darkness under -20^{o}C (Suzuki & Ishimaru, 1990) and Chl-a quantified using a pre-calibrated fluorometer (10-AU, Turner Design, USA). A second aliquot of 5 mL for nitrate + nitrite (NO_x^-), phosphate (PO_4^{3-}) and silicate (DSi) analyses was stored at -20°C until later analysis using an automated nutrient analyzer (AACS-IV, BL-TEC, Japan and TRAACS 2000, Bran+Luebbe, Germany). Detection limits based on this approach were 0.1, 0.08 and 0.1 μM for NO_x^-, PO_4^{3-} and DSi, respectively.

Phytoplankton particulate absorption coefficients, $a_{ph}(\lambda)$ (m^{-1}), were determined from a 500 mL aliquot using the quantitative filter technique of Cleveland & Weidemann (1993) as adapted by Wang *et al.* (2014). Wavelength resolved phytoplankton absorption spectra were determined as $a_{ph}(\lambda) = a_p(\lambda) - a_{np}(\lambda)$; where a_p and a_{np} refer to total particulate material and non-phytoplankton particles. The Chl-a specific absorption coefficient, $a_{ph}^*(\lambda)$ (m^2 mg Chl-a $^{-1}$), was then calculated as $a_{ph}(\lambda)$ normalised to the corresponding Chl-a concentration.

An additional aliquot of 1 L water samples were again filtered onto 25 mm GF/F filters under low vacuum pressure (< 0.02 MPa), and immediately frozen in liquid nitrogen and stored at -80^{o}C for later laboratory analysis. Samples were analysed by reverse-phase HPLC with a Zorbax Eclipse

XDB-C8 column (150 mm × 4.6 mm, 3.5 μm; Agilent Technologies), and 19 pigments were separated and quantified following the method of Van Heukelem and Thomas (2001).

Measurements of carbon uptake were carried out via 24 hours on-deck simulated-in-situ (SIS) incubations with enrichment of ^{13}C stable isotope (min 98 atom%; $NaH^{13}CO_3$, ISOTEC), where the final ^{13}C atom % of total dissolved inorganic carbon was ca. 10% of that in the ambient water (Hama et al. 1983). Sampling depths for incubation corresponded to 100, 50, 25, 10, 5 and 1% of PAR measured just below the sea surface (E_0^-), which were determined by PRR-800 measurements one day before at the same location. Incubators that simulated the irradiance levels from 50% to 1% of surface values were covered with blue plastic filters (The General Environmental Technos, Japan) to achieve the desired irradiances (no filter was used for 100% PAR incubator). Sampling, experimental procedures and in-lab measurements were the same as described previously by Tripathy (2010) and Zhu et al. (2016), except that the sampling volume was 1 L for this region. Finally, carbon fixation rates ($P^C(z)$) were calculated according to Hama et al. (1983) as follows:

$$\mathrm{P} = \frac{\Delta C}{t} = \frac{C \times (a_{is} - a_{ns})}{t \times (a_{ic} - a_{ns})} \quad (1)$$

where P is the photosynthetic rate (mgC m^{-3} d^{-1}), t is the time of incubation in hours (for our study was 24h), C is particulate organic carbon (POC) in the incubated sample (mgC m^{-3}), ΔC is POC increase during the incubation (mgC m^{-3}). Also, a_{is} is the atomic % of ^{13}C in the incubated sample, a_{ns} is the atomic % of ^{13}C in the natural sample, a_{ic} is the atomic % of ^{13}C in the total inorganic carbon. All ^{13}C data (P; Eq. 1) was subsequently spectrally corrected to account for the differences between light spectra for the incubators versus those *in situ*. For this, values of P were adjusted by the ratio, $\bar{a}^{chl}(in\ situ)/\bar{a}^{chl}(incubator)$, where $\bar{a}^{chl}(incubator)$ and $\bar{a}^{chl}(in\ situ)$ represent the phytoplankton absorption coefficients weighted to the irradiance spectra in each incubator and irradiance spectra *in situ*, respectively. Chl-a specific primary productivity ($P_B^C(z)$)

was calculated as $P^C(z)$ divided by Chl-a concentration, and the water column integrated P^C (PP_{eu}) was derived as $\int_0^{\mathrm{Zeu}} P^C(z)\mathrm{dz}$.

Phytoplankton pigment-based size fractionation

In order to consider the taxonomic nature of the phytoplankton community, we employed diagnostic pigment (DP) analysis following Vidussi et al. (2001) and Uitz et al. (2006) to estimate the respective contribution of three phytoplankton size classes: pico- (<2 μm), nano- (2-20 μm) and micro-phytoplankton (>20 μm) to total Chl-a (Tchla) biomass. Their approach uses seven biomarker pigments (fucoxanthin (Fuco), peridinin (Per), 19'-hexanoyloxyfucoxanthin (Hex), 19'-butanoyloxyfucoxanthin (But), alloxanthin (Allo), chlorophyll b (Chlb), and zeaxanthin (Zea)). Hirata et al. (2008) further revised the approach to account for the occurrence of Chl *b* in larger eukaryotes such as chlorophytes. We therefore followed Hirata et al. (2008), subsequently adapted by Wang et al. (2014) for phytoplankton size fraction analysis for the same region as in our study. The fraction of each size class was expressed as:

$$f_{micro} = (1.41\mathrm{Fuco} + 1.41\mathrm{Per})/\sum\mathrm{DP} \quad (2)$$

$$f_{nano} = (0.60\mathrm{Allo} + 0.35\mathrm{But} + 1.27\mathrm{Hex} + 1.01\mathrm{Chlb})/\sum\mathrm{DP} \quad (3)$$

$$f_{\mathrm{pico}} = 0.86\mathrm{Zea}/\sum\mathrm{DP} \quad (4)$$

$$\sum\mathrm{DP} = 1.41\mathrm{Fuco} + 1.41\mathrm{Per} + 0.60\mathrm{Allo} + 0.35\mathrm{But} + 1.27\mathrm{Hex} + 1.01\mathrm{Chlb} + 0.86\mathrm{Zea} \quad (5)$$

where coefficients for $\sum\mathrm{DP}$ follow Wang et al. (2014). Based on their approach, f_{micro}, f_{nano} and f_{pico} represents the fraction of relatively large diatoms and dinoflagellates, relatively smaller prymnesiophytes, chrysophytes, cryptophytes and chloropytes, and for fraction of cyanobacteria only, respectively.

FRRf measurements, ETR and K_C

In parallel with the 24h deck-board ^{13}C-uptake measurements and the *in situ* multispectral irradiance profiles, we also conducted FRRf fluorescence profiles measurement every 2 hours from dawn to dusk (as per Zhu et al. 2016). For 3 of the sampling campaigns, these diurnal FRRf profiles could only be conducted for half the daylight period and therefore are treated separately, as described below. Fluorescence inductions were performed semi-continuously from the near surface (~1 m deep) to depths >Z_{eu} using a Diving Flash Fast Repetition Rate fluorometer (FRRf, Kimoto Electric, Japan). The instrument is equipped with both dark and light chambers as well as an integrated scalar PAR sensor (QSP-2200, Biospherical Inc.). FRRf was deployed with an initial 1 min stop at the surface and a subsequently low profiling speed (<0.2 m s^{-1}) to ensure acquisition of fine scale surface and vertically resolved active fluorescence data (as per Mino et al. 2014). Settings for each FRRf induction acquisition followed Fujiki et al. (2008). Each induction transient was then fitted to the biophysical model of Kolber et al. (1998) to determine the minimum fluorescence yield, maximum fluorescence yield, effective absorption and photochemical efficiency of photosystem II (PSII) from both dark (F_o, F_m, σ_{PSII} and F_v/F_m) and light (F', F_m', σ_{PSII}' and F_q'/F_m') chambers (Table 2), using custom software (FRRCalc2, Kimoto Electric, Japan). From these FRRf parameters, and in concert with the *in situ* and on deck irradiance measurements, we used the approach of Zhu et al. (2016) to determine the daily-integrated ETR. Firstly, we calculated the instantaneous PSII reaction centre (RCII) normalised ETR, ETR_{RCII} (mol e^- mol $RCII^{-1}$ s^{-1}) per depth (z, m) and measurement time (t, h) from the FRRf profiles as,

$$\mathrm{ETR}_{RCII}(\mathrm{z},\mathrm{t}) = \mathrm{PAR}(\mathrm{z},\mathrm{t}) \times \sigma_{PSII}^{470}(\mathrm{z},\mathrm{t}) \times q_p(\mathrm{z},\mathrm{t}) \times \Phi_{RC} \times 6.022 \times 10^{-3} \quad (6)$$

where PAR is in units of μmol quanta m^{-2} s^{-1} and σ_{PSII}^{470} is the spectrally uncorrected effective

absorption cross section of PSII from the dark chamber ($Å^2$ $quanta^{-1}$). Note that under ambient light conditions, σ_{PSII}^{470} from the dark chamber accounts for any non-rapidly reversible (>s) non-photochemical quenching associated with the antennae (e.g. Suggett et al. 2006a, b). Φ_{RC} accounts for the assumption that one electron is produced from each RCII charge separation (see Kolber & Falkowski 1993). The constant value 6.022×10^{-3} converts µmol quanta to quanta, RCII to mol RCII and $Å^2$ to m^2. Finally, the term q_p (dimensionless) is the PSII operating efficiency and accounts for the extent of photochemical energy conversion by RCIIs, determined as the ratio of apparent PSII photochemical efficiency measured in 'light' and 'dark' chamber of the FRRf, following the procedure of Suggett et al. (2006a, b),

$$q_p = \frac{(F_{max}-F_{min})/(F_{max}-f)^{light\ chamber}}{(F_{max}-F_{min})/(F_{max}-f)^{dark\ chamber}} \quad (7)$$

Importantly this procedure overcomes the need to correct the PSII efficiency with knowledge of a fluorescence blank since the contribution of the blank (*f*) will be identical for both light and dark chambers and thus cancel (Suggett et al. 2006a).

We next constructed an ETR_{RCII} versus PAR relationship for each of the six light depths used for the corresponding incubations from profiles conducted across each sampling day (6-7 casts per day). Here, ETR_{RCII} and PAR data was binned per light depth and fit to the photosynthesis-light dependency model of Jassby & Platt (1976), Eq. 8. For the 3 campaigns where data was collected during half of the daylight period only, the ETR_{RCII} versus PAR relationship was constructed by combining profiles data from all 3 FRRf casts together and applied to each of the six depths. In this way we were also able to get a general ETR_{RCII} - PAR relationship for sampling campaigns where not enough FRRf data were obtained for depth-specific ETR_{RCII} - PAR curve construction.

$$ETR(z,t) = ETR_{max} \times \tanh(\frac{\alpha PAR(z,t)}{ETR_{max}}), \quad (8)$$

For waters where light saturation for ETR_{RCII} versus PAR was not observed, and hence ETR_{RCII}

remained light dependent, simple linear regression was instead used to describe the light-dependency of ETR_{RCII} (i.e. the slope is equivalent to α). Relationships between ETR_{RCII} and PAR for samples obtained under light-saturation and light-limiting conditions are provided in Fig. S1 as examples. Using knowledge of α and/or ETR_{max}, we were then able to retrieve the ETR_{RCII} for any given value of PAR over depth and time.

PAR(z,t) was specifically determined for our 6 sampling depths and derived from continuously measured incident PAR at the surface $PAR(0^+)$. The factor 0.9 was used to convert PAR above the water surface relative to that just beneath the surface ($PAR(0^-)$; see Marra, 2015). In water PAR at the % light depth of interest (x%) could be determined as $PAR(0^-)(t) \times$ x% (see Zhu et al. 2016). Knowledge of PAR(t,z) could then be applied to equation 5 to retrieve ETR for the given depths and time, ETR(z,t). Daily integrated ETR_{RCII} (mol e^- mol $RCII^{-1}$ d^{-1}) for each specific depth was finally determined as:

$$daily\ ETR_{RCII}(z) = \int_{t1}^{t2} ETR_{RCII}(z,t)dt \quad (9)$$

In order to convert ETR normalised to RCII content (ETR_{RCII}) to that normalised to Chla content, and hence ETRs that could be directly compared with parallel measures of carbon uptake to retrieve K_C (Lawrenz et al. 2013) knowledge of the RCII per Chl-a (i.e. n_{PSII}, mol RCII [mol Chl-a]$^{-1}$) is required. Direct measurement of n_{PSII} under natural conditions is extremely challenging (Suggett et al. 2006a, Moore et al. 2006) often requiring that the RCII concentration be determined indirectly (see Suggett et al. 2010). Based on previously published information, we employed an approach to determine n_{PSII} based on phytoplankton taxonomic size class information. We summarized n_{PSII} from 11 phytoplankton species under various growth conditions (reported by Suggett et al. 2004) and grouped this dataset into two size communities; <2 µm (cyanobacteria) with n_{PSII} of 0.0038 ± 0.00004 mol RCII [mol Chl-a]$^{-1}$ and >2 µm (other eukaryotes) with

average n_{PSII} of 0.0017 ± 0.00003 mol RCII [mol Chl-a]$^{-1}$, respectively. Thus, n_{PSII} was calculated based on size fraction derived from HPLC, using following equation:

$$n_{PSII} = \%(Micro + Nano) * 0.0017 + \%(Pico) * 0.0038 \quad (10)$$

Measurements of σ_{PSII} were weighted to the narrow blue excitation waveband (470 nm) used for fluorescence induction by the FRRf. To therefore account for the spectral differences between FRRf-LEDs and the natural light spectra *in situ*, we employed a σ_{PSII}-correction factor (F) according to Eq. 11 following Suggett et al. (2006b):

$$F = \sigma_{PSII}^{abs} / \sigma_{PSII}^{470} = (\frac{\bar{a}^{chl}(in\ situ)}{\bar{a}^{chl}(FRRf)}), \quad (11)$$

where σ_{PSII}^{abs} represents spectral corrected σ_{PSII}; $\bar{a}^{chl}(FRRf)$ and $\bar{a}^{chl}(in\ situ)$ represent the absorption coefficients weighted to the FRRf excitation spectra and *in situ* irradiance spectra, respectively. Detail calculations for $\bar{a}^{chl}(FRRf)$ and $\bar{a}^{chl}(in\ situ)$ can be found in Suggett et al. (2004) and Zhu et al. (2016). A daily Chl-a specific ETR at light depth (z) (mmol e$^-$ mg Chl-a^{-1} d^{-1}) was thus calculated as follows:

$$daily\ ETR(z) = daily\ ETR_{RCII}(z) \times n_{PSII} \times F \times 893^{-1} \quad (12)$$

where, the constant factor 893 converts mol Chla to mg Chla and mol e$^-$ to mmol e$^-$.

Finally, K_C (mol e$^-$ (mol C)$^{-1}$) was defined to be the ratio of the two independently determined variables, ETR and P_B^C as per Zhu et al. (2016):

$$K_C(z) = \text{daily } ETR(z)/P_B^C(z) \times 12 \quad (13)$$

where P_B^C is the daily-integrated carbon assimilation per unit Chl-a (mgC mg Chl-a^{-1} d^{-1}), and the factor 12 converts g C to mol C.

Statistical analyses

Hierarchical cluster analysis (HCA) was applied to physico-chemical parameters across sampling campaigns for grouping into common hydrographic conditions and "ward.D2" method in R was adopted for running HCA, which using euclidean distances as input dissimilarities (Murtagh & Legendre, 2014). Spearman rank correlation analysis and stepwise regression were utilized to examine contribution of physico-chemical (or taxonomic) variables in explaining variance of K_C. Kolmogorov Smirnov test was used to examine data normal distribution. Welch t-test and ANCOVA were applied for testing significant difference between clusters or groups data and the linear regression models. All statistical analyses and curve fitting were performed using open source statistical software R version 3.2.3 (R Core Team, 2014).

RESULTS

Variability of carbon uptake rates, electron transport rates, and K_C

Volume normalized carbon uptake rates ($P^C(z)$, mgC m^{-3} d^{-1}) across all sampling campaigns were generally higher for the ECS mid-shelf than for ECS outer shelf and TS waters (Table 3), and reflected that phytoplankton biomass was also higher for the ECS mid shelf than ECS outer shelf/TS. Specifically, surface mean P^C and Chl-a was ca. 10 times (upper mixed layer) or 4 times (deep chlorophyll a maxima, DCM) higher for the ECS mid-shelf than the ECS outer-shelf/TS, whereas values for Chla-normalised P^C (P_B^C(z)) were generally equivalent across sites for both the upper mixed layer (ca. 40 mgC mg Chl-a^{-1} d^{-1}) and DCM (ca. 20-30 mgC mg Chl-a^{-1} d^{-1}). Euphotic depth integrated P^C (PP_{eu}) values ranged from 330 to 1250 mgC m^{-2} d^{-1} across the study area, but overall higher for the ECS mid-shelf with (mean ± standard error (SE), 853 ± 97 mgC m^{-2} d^{-1}) compared to ECS outer-shelf/TS (451 ± 51 mgC m^{-2} d^{-1}).

311 Significant variability of ETR_{RCII} was observed over the course of the diurnal cycle, with
312 patterns of ETR_{RCII} closely coupled with surface PAR over time (e.g. ETR_{RCII} of surface and DCM,
313 Fig. 2); as expected, this ETR_{RCII} variability was dampened at depth (DCM) as a result of the lower
314 light availability. Thus for any given light depth, values of daily integrated ETR(z) were therefore
315 closely correlated with those of daily integrated PAR(z) across all sampling campaigns ($R^2 = 0.93$, n
316 = 72, $p < 0.001$), with a maximum value of ca. 170 mmol e^- (mg Chl-a)$^{-1}$ d^{-1} (Fig. 3a) from across
317 the entire dataset. In contrast, greater non-linearity (and in effect, daily light saturation) was
318 observed when parallel values for the daily-integrated rate of carbon uptake (P_B^C(z)) were plotted
319 against PAR(z) (Fig. 3b). Given the respective patterns of light dependency for (P_B^C(z)) and ETR(z),
320 further plotting P_B^C(z) against corresponding values of ETR(z) highlighted non-linearity between
321 corresponding data points (Fig. 3c) and thus a clear indication that the electron requirement for C
322 fixation (K_C, ETR(z)/P_B^C(z)) was not constant. Overall, K_C (mol e^- [mol C]$^{-1}$) ranged from values of
323 1.0 to 66.5 mol e^- (mol C)$^{-1}$, similar to values reported for a previously synthesised global K_C
324 dataset (Lawrenz et al. 2013).

325 Of our 67 K_C data points, 8 values (primarily from PAR depths of 5% and 1% E(0^-)), were
326 below the theoretical minimum of 4 mol e^- (mol C)$^{-1}$. K_C values <4 have been previously observed
327 for laboratory cultures under controlled conditions but only where ambient light levels are lowest.
328 Therefore, considering the low values of P_B^C at these light depths (mean ± standard deviation (SD),
329 11.6 ± 10.2 mgC mg Chl-a^{-1} d^{-1}) and their relatively small proportion to the whole dataset, we
330 excluded K_C values <4 mol e^- (mol C)$^{-1}$ from further analysis, as a result of possible inaccuracies
331 associated with very low light C-uptake rates (Cullen 2001) or errors in n_{PSII}. With the exclusion
332 of these 8 data points, K_C varied from 4.3 to 66.5 mol e^- (mol C)$^{-1}$ with the mean ± SD of 19.8 ±
333 14.2 mol e^- (mol C)$^{-1}$.

Resolving variability of K_C via changes in light intensity

Spearman rank analysis of K_C for different environmental factors yielded PAR with the highest correlation coefficient with K_C (Spearman, r = 0.82, p < 0.001, Table S1). Stepwise regression further confirmed that PAR alone explained most (66%) of K_C co-variability (Table S2). PAR was therefore considered to be the main factor explaining the variability of K_C for this region. Indeed, variability of K_C for the entire dataset could therefore be described by one simple PAR dependent linear model (K_C = 0.85PAR + 6.55, R^2 = 0.66, n= 59, p < 0.001, Fig. 3d) as we have demonstrated previously for Ariake Bay (Zhu et al., 2016). We further considered whether K_C variability was different for (high light) upper mixed layers compared to the (lower light) other depths. Binning K_C values into these two sample groups demonstrated that K_C was higher and much more variable in the upper mixed layer (mean ± SE, 31.2 ± 3.3 mol e^- $(mol\ C)^{-1}$) compared to the other depths (13.2 ± 1.1 mol e^- $(mol\ C)^{-1}$) (see Fig. 3d).

Resolving variability of K_C via changes in phytoplankton community structure

Sampling stations analysed by HCA based on prevailing physico-chemical features (sea surface temperature, salinity and nutrients (NO_3^-+NO_2^- , PO_4^{3-}), water column mixed layer depth (MLD) and mean light diffuse attenuation K_d(PAR)) yielded two main groups (Fig. 4a). Specifically, stations were clustered (cluster "A", most located in the outer shelf and TS) with higher salinity, lower nutrient and Chl-a concentration compared to all other stations ("cluster "B") (Table 4). Analysis of the phytoplankton community structure revealed dominance by f_{micro} (%, mean ± SE, 41.2 ± 6.3) or f_{pico} (45.7 ± 7.5) for stations comprising clusters A and B, respectively (Table 4). However, these two clusters also exhibited similar proportions of f_{nano} (43% versus (vs.) 32%, respectively). Mean (± SE) values for K_C at within this high light upper mixed layer was similar for

data binned according to these two clusters (28.74 ± 1.6 (n = 10) vs. 34.1 ± 4.2 mol e^- $(mol\ C)^{-1}$, n = 16) (Table 4). Based on this HCA result, we plotted PAR(z) versus K_C(z) for these two clusters separately to further examine the potential influence of environmental condition on the light-dependency of K_C (Fig. 4b). Here, the correlation between K_C(z) and PAR(z) was improved (R^2 = 0.74, Fig. 4b) for both clusters compared to that previously where all data was pooled (R^2 = 0.66, Fig. 3d). Furthermore, Cluster B data exhibited a significantly higher regression slope than for cluster A (1.1 vs. 0.55, ANCOVA, df=1, $p < 0.001$) (Fig. 4b).

Given the substantial overlap of phytoplankton group dominance between physico-chemical defined clusters (and the focus on only the upper mixed layers), we subsequently re-binned all data across all campaign/depth according to dominant phytoplankton fraction. This approach yielded dominant phytoplankton size groups (f_{micro}-, f_{nano}- and f_{pico}-dominated) consisting of 26, 20 and 13 data points, respectively (Table 5). Mean K_C (z) was again effectively constant (ca. 16-22 mol e-$(mol\ C)^{-1}$ across these three phytoplankton size bins (Table 5), although median K_C(z) values were generally higher for f_{pico} compared to f_{nano} or f_{micro} (ca. 18 compared to ca. 15 or 12, Fig. 5a). Such higher K_C values for f_{pico} dominated waters may be a function of the higher n_{PSII} values ascribed to these waters (Suggett et al., 2004), or the higher light intensity since most f_{pico} dominated waters were at surface (Lawrenz et al., 2013). Re-evaluating the relationship of K_C (z) versus PAR (z) in terms of these three size bins (Fig. 5b), improved the extent of covariance that could be explained (R^2 = 0.59-0.81, $p < 0.001$) compared to the pooled data (Fig 3d) or, in the case of f_{micro} and f_{pico}, compared to the two physico-chemical based clusters (Fig. 4b). ANCOVA analysis demonstrated that the regression slopes describing relationship between K_C and PAR for f_{micro} was significantly different than for f_{nano} and f_{pico} (df=1, $p < 0.001$) but not for f_{nano} compared to f_{pico} (df=1, p = 0.2) (Fig. 5b). Thus, data from f_{nano} and f_{pico} bins were pooled for final analysis.

379 Overall, the linear regression slope of K_C (z) versus PAR (z) was ca. a factor of 2 higher for samples
380 dominated by micro-phytoplankton (i.e. f_{micro} >20 µm, determined by pigments of Fuco and Per)
381 than those dominated by small phytoplankton (f_{nano} + f_{pico}, <20 µm, determined by pigments of Hex,
382 But, Allo, Chlb, and Zea) (slope: 1.2 vs. 0.56, ANCOVA, df=1, $p < 0.001$). Considering the data as
383 these two different taxonomic groups demonstrated improved correlation between K_C (z) and PAR(z)
384 (R^2, 0.70-0.81 Fig. 5c) compared to physico-chemical defined clusters (0.74, Fig. 4b), suggesting
385 that K_C appears primarily influenced by light and secondarily by dominant phytoplankton taxa
386 present. These improved regression coefficients for taxonomic-based groups suggest that
387 accounting for differences in phytoplankton community composition is therefore important in these
388 waters for improving light-dependent estimations of K_C across broad environmental regimes such as
389 those seen here in the East China Sea.
390

DISCUSSION

Studies are increasingly demonstrating that FRRf-based ETRs couple well with C-uptake rates (e.g. Lawrenz et al. 2013, Schuback et al. 2015), but that the exact relationship between rates varies with environmental condition (Lawrenz et al. 2013), as we also recently observed for waters of Ariake Bay (Zhu et al., 2016) and for our current study. Our study differs from many previous works exmaining variance of K_C (e.g. reviewed in Lawrenz et al. 2013) where carbon uptake was determined from ^{14}C uptake typically over 1-2 hour incubations, and thus presumably closer to gross carbon uptake (GPP), whereas we utilised ^{13}C uptake over 24-hour incubations (i.e. net production, NPP). This differentiation is important where Halsey et al. (2010, 2011) note that K_C measurements based on net C production measurements are more tightly coupled than those based on gross C production measurements across gradients of varying nutrient availability. In our current study we observed that light appears to be most associated with deviation of K_C from the theoretical minimum value of 4 mol e^- mol C^{-1} (Fig. 6), as previously observed for another region using the same approach (Ariake Bay, see Zhu et al., 2016); however, we further demonstrate that in fact phytoplankton taxonomic structure, which in part is inherently tied to changes in physico-chemical condition (see also Suggett et al. 2006a), appears an important contributor to variability of K_C over broad scales. In the following sections, we discuss these findings and how they provide a means to estimate K_C (and hence net carbon uptake from FRRf) in the ECS and TS regions.

Light and phytoplankton community effects on K_C variability

Values of K_C for our current study (summer season of eastern ECS and TS) varied from 1.0 to 66.5 mol e^- $(mol\ C)^{-1}$ (mean ± SD of 18.2 ± 16.6, n = 67). Whilst this range of values is somewhat

higher than that recently reported for Ariake bay (2.3-26.6, Zhu et al. 2016), it is within that previously reported from a global assessment covering broad biogeographic environments (1.15-54.2 mol e^- (mol C)$^{-1}$, mean: 10.9 ± 6.91; Lawrenz et al. 2013), where higher values were characteristic of waters subjected to nutrient stress and/or limitation. As with many previous FRRf-based studies (Corno et al. 2006, Melrose et al. 2006, Suggett et al. 2006a, 2009a), some values for K_C lower than the theoretical minimum (4 mol e^- (mol C)$^{-1}$, see Kolber & Falkowski 1993) were observed, but only for deeper waters with extremely low light intensities. Low values for K_C (<4 mol e^- (mol C)$^{-1}$) have been observed in culture (2.68-3.79 mol e^- (mol C)$^{-1}$, Suggett et al., 2009a, Hoppe et al., 2015) and *in situ* (e.g. 0.24-2.46 mol e^- (mol C)$^{-1}$, Robinson et al., 2014), and generally considered an overestimation of carbon uptake and/or underestimation of ETR (Suggett et al. 2009a, Lawrenz et al. 2013) particularly when cyanobacteria are present (see Simis et al. 2012, Robinson et al. 2014). Furthermore, the lowest values of K_C we observed were all from deep waters where ambient light levels were lowest. As such, it is likely that low values of K_C may have been driven by inaccurate C uptake measurement (overestimation) for samples from low photic zones (Cullen, 2001), or not accounting for inherent diurnal variability for n_{PSII} that may cause underestimate in ETR (Schuback et al., 2016). However, we cannot further discount possible additional overestimation of C uptake where these deeper (low light) samples were also incubated at higher temperatures than ambient as a result of on-deck incubations using surface water for temperatures control. Here, average temperature differences between the upper mixed and deep layers (1% and 5% surface light depths) was ca. 8.5°C, which can cause as much as 40% overestimate of carbon uptake rate (Davison, 1991).

K_C values in excess of 4 mol e^- (mol C)$^{-1}$ is reflective of ETRs that are decoupled from C-fixation (Lawrenz et al. 2013), in particular as cellular demands for energy (ATP) and reductant

435 (NADPH) from processes other than C fixation increase (see Suggett et al. 2009a, 2010). In our
436 present study, we observed the decoupling of ETRs from C-uptake in particular at high irradiances,
437 also consistent with the recent observations across a broad range of biogeographic areas (Schuback
438 et al. 2015, 2016), an Arctic fjord (Hancke et al. 2015) and a semi-closed embayment (Zhu et al.
439 2016). Intensity of the ambient light field appears to be a dominant environmental factor associated
440 with decoupling of ETR from PP in our present study (Fig. 3d, 6). This outcome is perhaps not
441 surprising since:

442 Firstly, equilibration of isotopic label through cellular pools pushes the PP estimate towards net
443 photosynthesis with longer incubations as recently-fixed ^{13}C is increasingly respired (i.e. dark loss;
444 Eppley & Sharp 1975). The magnitude of loss can be very high, particularly at high irradiance, and
445 can be dependent on nutrient status (Halsey et al. 2014), and thus potentially explain the
446 irradiance-dependent increase in K_C we observed; and secondly, mechanisms such as
447 photoprotection act to dissipate electrons/consume O_2 without necessarily impacting on CO_2 once
448 light intensity exceeds that required to saturate photochemistry (e.g. Schuback et al. 2015).
449 Maximum turnover rates of the electron transport chain (ETC) require that excess excitation energy
450 be dissipated as thermal energy in the PSII antenna (known as non-photochemical quenching, NPQ)
451 in order to avoid photoinhibtion. Indeed, NPQ has been observed to highly correlate with
452 $K_C/\ n_{PSII}$ (Schuback et al. 2015, 2016, 2017), which may result from the progressive
453 photoinactivation of n_{PSII} with increasing irradiance (Behrenfeld et al. 1998), or the co-response to
454 excess excitation pressure for both NPQ and K_C/n_{PSII} (Schuback et al. 2016). In order to account for
455 any such changes in n_{PSII} (and simultaneously address whether use of a constant for n_{PSII}
456 potentially introduced error into ETR and hence K_C), we repeated a diurnal analysis of relative
457 $1/n_{PSII}$ as per Schuback et al (2016). For this, we examined F_o/σ_{PSII} as the factor describing

458 n_{PSII} stability (Oxborough et al. 2012). Results showed that difference of n_{PSII} with time of day
459 were not significant for 7 of 12 cruises (Welch t-test, table S3). Thus n_{PSII} remains somehow
460 constant with time of day and does not likely exhibits very large diurnal variance in our study.
461 (Table S3), suggesting other processes must account for our light dependency of K_C.

462 High electron transport (but low carbon assimilation) can be sustained via up-regulation of
463 alternative electron flow after charge separation at PSII. For example, plastoquinol terminal oxidase
464 (PTOX) uses electrons from the plastoquinone pool to reduce oxygen and thus protect PSII
465 acceptors from high light damage (reviewed by Cardol et al. 2011). Electron passed to photosystem
466 I can be used to further reduce oxygen by Mehler activity (Mehler 1951, Roberty et al. 2014). As a
467 result, C fixation rates saturate with lower irradiances than ETRs (Mackey et al. 2008, Schuback et
468 al. 2017) and hence decoupling between ETRs and C-upatke would be expected to enlarged as
469 irradiance continues to increase above that for light saturation (E_K). Consequently, on balance,
470 photoprotective processes would likely provide a rationale as to why K_C often varies with light
471 availability. However, it should be noted that our study considers daily-integrated ETR and P_B^C, and
472 hence mechanisms acting to decouple these two rates (and hence K_C) must ultimately reflect the
473 outcome of longer term photo-acclimation processes.

474 Previous studies have indicated light-dependency of K_C from field evidence, where low light
475 conditions associate with lower K_C values (see Lawrenz et al. 2013), and laboratory experiments on
476 microalgae (Suggett et al. 2008, 2010, Brading et al. 2013). However, strong covariance of K_C with
477 PAR was not demonstrated until Zhu et al. (2016) for Ariake Bay. That said, as compared to our
478 previous observations of (Zhu et al. 2016; their Fig. 9c), a relatively large proportion of variance for
479 K_C could not be explained by PAR, notably at high daily PAR values (Fig. 3d), confirming that
480 factors other than light regulation are also responsible for variations in K_C (e.g. Suggett et al. 2006a,

Lawrenz et al. 2013, Schuback et al. 2015).

Adaptive differences in energy and reductant demands to maintain growth optima would explain observations of K_C variability within a relatively small range; specficially, previous laboratory experiments under controlled growth conditions report K_C with a range of ca. 5-15 across diatoms, flagellates and chlorophytes (Suggett et al. 2009a, Brading et al. 2013); these values remain lower than those reported for our natural samples (4.3 to 66.5 mol e^- (mol C)$^{-1}$), but generally within a similar range reported by Schuback et al. (2015, 2016) for a diatom and prymnesiophyte (ca. 6 to 20 mol e^- (mol C)$^{-1}$) assuming a value for $1/n_{PSII}$ of ca. 650 versus 1325 mol Chla (mol RCII)$^{-1}$ for iron replete versus limited eukaryotes (see Silsbe et al. 2015). Although the East China Sea is not under iron limitation, we observed a higher range of K_C than compared to those of Schuback et al. (2015, 2016) in the iron limited Pacific. There are two main reasons that probably can explain this difference; firstly, we agree that the nutrient level could influence K_C value and K_C will likely be elevated under conditions of nutrient stress/starvation (Lawrenz et al. 2013). However, both Schuback et al. (2015, 2016) and our studies (Zhu et al. 2016 and this study) suggested that K_C appears primarily influenced by light intensity (presented as NPQ in Schuback et al (2015, 2016)); thus, the larger K_C values found in our surface data probably relates to the higher daily PAR included in this study (40-60 mol quanta m^{-2} d^{-1} vs. ca.30 mol quanta m^{-2} d^{-1} in Schuback et al.). Secondly, the different incubation time that two studies applied for may also cause our higher K_C value. Specifically, longer incubating time (24 h, i.e. NPP) of our study than for Schuback et al. (3-4 h, i.e. GPP) probably results our lower primary productivity thus higher K_C presented here. Our high values for K_C (>15-20 mol e^-(mol C)$^{-1}$) occur almost exclusively where PAR was highest (>20 mol quanta m^{-2} d^{-1}), reinforcing the notion of high light in moderating the cellular demands of energy/reductant (and the need to consume 'excess' electrons and/or O_2). However, most

504 importantly this light-dependency is different for our f_{micro} compared to f_{nano} + f_{pico} fractions (Fig.
505 5c), whereby the higher linear regression slope for f_{micro} suggests that high light decoupling of ETRs
506 and C-uptake appears more severe for diatoms/dinoflagellates (fucoxanthin and peridinin dominated
507 communities) compared to nanoflagellates (19'-hexanoyloxyfucoxanthin,
508 19'-butanoyloxyfucoxanthin, alloxanthin and chlorophyll b) and cyanobacteria (zeaxanthin)
509 dominated communities.

510 Whilst higher values of K_C for f_{micro} would seem to contrast with previous observations where
511 K_C typically remains low for diatom (and flagellate) dominated waters (e.g. Suggett et al. 2006a),
512 we can potentially explain these higher values from one or more factors: Differences in light
513 absorption efficiency and electron transport between phytoplankton groups no doubt enhance
514 ETR_{RCII} variability to a certain degree (see Giannini & Ciotti (2016)). The higher K_C values
515 observed for larger phytoplankton in our study implies that energy transfer efficiency from
516 photochemistry to biomass production is lower for large phytoplankton. However, the fact that
517 highly effective photoprotection mechanisms appear to operate in both large (e.g. diatom, especially
518 for those living in dynamic waters; Lavaud et al. 2002, 2007; Hoppe et al. 2015) and small (Dimier
519 et al. 2007, 2009) phytoplankton taxa, as well as highly conserved ETR (z) versus PAR (z) (Fig. 3a)
520 across depths/campaigns in our study, would suggest that taxonomic differences associated with
521 light harvesting (and importantly dissipation) do not likely contribute to the differences observed
522 for K_C. Instead, differences in P_B^C (carbon fixation) appear to play a key role (Fig. 3b, Table 6).

523 Lower size-normalised photosynthetic rates for large size phytoplankton have frequently been
524 reported (Malone, 1980, Montecino & Quiroz, 2000, Bouman et al. 2005, Kameda & Ishizaka 2005,
525 Tripathy et al. 2014, Barnes et al. 2015) and explained by lower surface-to-volume ratio of larger
526 phytoplankton reducing nutrient uptake efficiency (Sunda & Huntsman, 1997) and light absorption

(Marra et al. 2007). Such constraints are thus compounded by nutrient limitation (Riegman et al., 1993, Pedersen & Borum, 1996). Whilst f_{micro} was generally dominant in waters with lower salinity and higher nutrients (cluster B, Fig 4a), nutrient concentrations were still overall very low (NO_x^-: ~0.5 μM; PO_4^{3-} : ~0.09 μM) and at concentrations in this region where phytoplankton generally appear to experience nutrient stress (Liu et al. 2013). However, higher values of P^B are more typical for large phytoplankton when under nutrient repletion conditions (Cermeño et al. 2005). Such overall nutrient limiting (starving) conditions may thus also explain the somewhat contrasting observations here compared to our recent study with Ariake Bay (Zhu et al. 2016) where nutrients were replete; specifically, phytoplankton in Ariake Bay exhibited higher P_B^C values (and thus lower K_C and lower regression slope value of K_C (z) versus PAR (z)) (Zhu et al. 2016) under similar light intensity as for our current study.

In addition, the high abundance of cyanobacteria in the f_{nano} + f_{pico} may have driven an overall lower value for K_C for this fraction compared to the f_{micro} (Robinson et al. 2014; see also Simis et al. 2012). Clearly, resolving which of these factors is at play is currently beyond our study and further highlights that more controlled experiments are required to disentangle the potentially confounding role of (non-steady state) environmental conditions and taxonomy upon K_C. Even whilst we cannot fully resolve the mechanisms driving the values of K_C within our current study, our data still demonstrates a clear role of taxonomy (or at least pigment group as in our study) in better accounting for variance of K_C across spatially and/or temporally separated samples.

Uncertainty assessment of the linear relationship between PAR and K_C

As with previous K_C-focussed studies, a large number of assumptions are employed in in particular for the FRRf-based ETRs (Lawrenz et al. 2013, Schuback et al. 2015). Whilst the strong

549 co-variation between K_C and light we observed here provides a potentially promising means to
550 easily retrieve K_C from future FRRf data, it is critical to first evaluate the possible error propagation
551 via the *a priori* assumptions used. Notably, the assumed constant value for n_{PSII} of 0.0038 for
552 picoplankton, which is high than that reported by Suggett et al (2004) for *Aureococcus* and
553 *Pycnococcus* (ca. 2 μm in diameter and a mean value of 0.0013 mol RCII [mol Chla]$^{-1}$). Also, the
554 correction method for σ_{PSII} based on absorption spectra rather than fluorescence excitation spectra
555 (see also Suggett et al. 2010), which in the latter case likely better accounts for the proportion of all
556 light absorbed by PSII especially for cyanobacteria (Suggett et al., 2004; Moore et al, 2006). In the
557 case of our parallel ^{13}C-uptake measurements, we acknowledge that the lack of dissolved organic
558 carbon (DOC) measurement in this study will underestimate P_B^C and thus overestimate K_C by ca.
559 2-50%, particularly at high irradiance (Thornton et al., 2014).

560 To consider such uncertainties, we therefore re-examined our light-*K*c relationship by randomly
561 introducing error estimates to each step: Firstly, we assumed a fraction of between 0 and 30% of
562 pico-phytoplankton is indeed eukaryotic (e.g. species of *Pycnococcus* and *Aureococcus*) rather than
563 cyanobacteria (*Synechococcus*) which would reduce n_{PSII} by ca. 0-20%. A random number
564 (chosen by R function runif()) within this 0-20% range of n_{PSII} was therefore subtracted from the
565 original value to simulate such uncertainty. Second, we assumed our σ_{PSII} correction factor F
566 would be overestimated ca. 0-20% because of using absorption spectra over fluorescence excitation
567 spectra in weighting of σ_{PSII} for cyanobacteria (Moore et al., 2006), and thus generated a random
568 number within this range. Third, in order to account for the underestimation of PP caused by the
569 lack of DOC measurements, the ratio of dissolved primary production to particulate primary
570 production (REP) was considered to be a value of 5-30% base on the nutrient conditions of study
571 area (Thornton et al., 2014). Particularly, 10-30% of the REP was added to P_B^C incubated under high

light (i.e. 100% and 50% surface light), whereas 5-10% error to P_B^C for all other samples accounting for a reduced REP proportion under lower irradiances (Thornton et al., 2014; Parker and Armbrust, 2005).

Uncertainty was thus determined as,

$$n_{PSII\ \text{simulated}} = n_{PSII\ \text{calculated}} - n_{PSII\ \text{calculated}} \times \text{x1\%}$$

$$F_{\text{simulated}} = F_{\text{calculated}} - F_{\text{calculated}} \times \text{x2\%}$$

$$P_{B\ \text{simulated}}^C = P_{B\ \text{measured}}^C + P_{B\ \text{measured}}^C \times \text{y\%}$$

where $\text{x1\%}$, $\text{x2\%}$ and $\text{y\%}$ are even distributed random numbers added to the parameters for accounting uncertainty of each.

Determination of uncertainty (simulation) totally repeated 100 times. The resultant K_C was calculated for each simulated ETR and P_B^C and compared against daily PAR, as per the original data. We then calculated the mean ± SD for each of the correlation coefficient (R^2), slope and intercept from the entire 100 simulations combined, which is 0.63±0.04, 0.54±0.04 and 4.6±0.3, respectively (i.e. K_C =0.54×PAR + 4.6 with R^2 = 0.63, P < 0.01). In comparison to our original data (K_C =0.85×PAR + 6.5 with R^2 = 0.66), the extent of covariance that can be explained by a linear model is broadly equivalent, but as expected changing the absolute terms with the ETR and ^{13}C equations significantly changes the slope. However, importantly in the case of our study, this uncertainty analysis confirms that a linear relationship between light and K_C is robust and highly repeatable depending on the choice of assumption used to generate the electron transport and carbon uptake rates. That said, future studies will need to move beyond use of these assumptions and the inherent uncertainty that is introduced.

Towards improved *in situ* application of FRRf-based K_C and NPP estimates

Our analysis here for the East China Sea (ECS) and Tsushima Strait (TS) (as well as that previously for Ariake bay; Zhu et al. 2016) have shown that variance of K_C can be reconciled with that of light availability. This outcome appears in agreement with previous data analyses from Lawrenz et al. (2013) who showed that K_C measurements from coastally influenced waters such as European shelf seas and the Baltic/Gulf of Finland could be modeled, in part, against optical depth and *in situ* light attenuation. Our data also confirms that knowledge of additional physico-chemical conditions is needed to effectively improve the robustness of these models (Fig. 4b). Lawrenz et al. (2013) highlight that a comprehensive description of physico-chemical conditions (temperature, salinity, nutrients etc.) is required to best explain variance of K_C. Whilst our analysis using taxonomic based clusters provided only slightly improved co-variance of K_C versus light, it arguably provides a more simplistic but powerful means to potentially predict K_C and hence NPP. Specifically, knowledge of fewer variables (in our case, phytoplankton size fractions based on pigment groups, as opposed to a salinity and nutrients that predominantly separated our stations) is required to bin K_C and light. Clearly, semi-continuous measurement of pigment groups needed to ensure the validity of FRRf across highly physically dynamic waters is not trivial. High throughput particle sensors may provide some means to retrieve phytoplankton size structure (Alvarez et al., 2011, 2014). However, our size based approach used knowledge of pigment groups. Thus parallel continuous measurements of light absorption (Ciotti et al., 2002, Wang et al., 2015), or better yet multispectral FRRf discrimination (Silsbe et al., 2015) may provide a means to identify taxonomic groups and their influence upon K_C.

In determining ETR_{RCII} and hence K_C (via ^{13}C-based daily integrated NPP estimates), we used

several assumptions. Specifically, algorithms describing (i) the spectral conversion of σ_{PSII} from the FRRf LEDs relative to the *in situ* light fields (Suggett et al. 2009b), and (ii) taxonomic weighting of n_{PSII}. The role of these assumptions in potentially influencing ETR has been reviewed extensively previously (e.g. Suggett et al. 2009b, 2010, Robinson et al. 2014); Even so, despite employing these assumptions, we demonstrated strong co-variance between K_C and environmental (and biological) factors thus providing a robust means to retrieve NPP across from future FRRf measurements for this region. In fact, such assumptions may not even be required where new FRRf based ETR models can remove the need for knowledge of n_{PSII} (Oxborough et al. 2012, Silsbe et al. 2015, Murphy et al. 2016; see also Schuback et al. 2015), and relatively small variability of the correction factor for σ_{PSII} with depth (Fig. S2) possibly suggesting that a single conserved correction factor could be employed with relatively little loss of accuracy. Such an outcome supports, at least in part, the notion that conversion of absorbed energy to net carbon fixation exhibits limited variability in the absence of non-photochemical quenching (Silsbe et al. 2016). Regardless of these future improvements, our study further evidence that FRRf-based ETRs can be reconciled with independent carbon uptake measurements, but for the first time through knowledge of phytoplankton groups. In doing so, we have produced a predictive algorithm for K_C for this ocean region opening possibilities of using FRRf-based platforms to examine carbon fluxes with improved resolution

Acknowledgements

We would like to thank the captain, officers and crew of T/V-Nagasaki Maru for their admirable assistance during onboard sampling and measurements. Many thanks to Dr. Koji Suzuki for measuring HPLC data. The earlier version of the manuscript has greatly benefited from the critical reading by Dr. Akiko Mizuno and Dr. Egil Sakshaug. We thank four anonymous reviewers for their very constructive comments and suggestions. This research was supported by the Global Change Observation Mission-Climate (GCOM-C) Project of Japan Aerospace Exploration Agency and partially supported by Japan Society for the Promotion of Science KAKENHI (JP26241009) and Zhejiang Provincial Natural Science Foundation of China (LQ16C030004). The contribution by Dr. David J. Suggett was supported by an Australian Research Council Future Fellowship (FT130100202); the contribution by Dr. Joaquim Goes was supported by the National Aeronautics and Space Administration (NNX16AD40G).

LITERATURE CITED

Álvarez E, López-Urrutia Á, Nogueira E, Fraga S (2011) How to effectively sample the plankton size spectrum? A case study using FlowCAM. J Plankton Res 33:1119-1133

Álvarez E, Moyano M, López-Urrutia Á, Nogueira E, Scharek R (2014) Routine determination of plankton community composition and size structure: a comparison between FlowCAM and light microscopy. J Plankton Res: 36:170-184

Barnes MK, Tilstone GH, Smyth TJ, Widdicombe CE, Gloël J, Robinson C, Kaiser J, Suggett DJ (2015) Drivers and effects of Karenia mikimotoi blooms in the western English Channel. Prog Oceanogr 137: 456-469

Brading P, Warner ME, Smith DJ, Suggett DJ (2013) Contrasting modes of inorganic carbon acquisition amongst Symbiodinium (Dinophyceae) phylotypes. New Phytol 200:432-442

Bouman H, Platt T, Sathyendranath S, Stuart V (2005) Dependence of light-saturated photosynthesis on temperature and community structure. Deep Sea Res I 52:1284-1299

Cardol P, Forti G, Finazzi G (2011) Regulation of electron transport in microalgae. Biochim Biophys Acta Bioenerg 1807: 912-918

Cermeño P, Estévez-Blanco P, Maranón E, Fernández E (2005) Maximum photosynthetic efficiency of size-fractionated phytoplankton assessed by ^{14}C uptake and fast repetition rate fluorometry. Limnol Oceanogr 50:1438-1446

Cheah W, Mcminn A, Griffiths FB, Westwood KJ, Wright SW, Molina E, Webb JP, Van Den Enden R (2011) Assessing Sub-Antarctic Zone primary productivity from fast repetition rate fluorometry. Deep Sea Res II 58**:** 2179-2188

Ciotti AM, Lewis MR, Cullen JJ (2002) Assessment of the relationships between dominant cell size

669 in natural phytoplankton communities and the spectral shape of the absorption coefficient.
670 Limnol Oceanogr 47: 404-417
671 Cleveland JS, Weidemann AD (1993). Quantifying absorption by aquatic particles: A multiple
672 scattering correction for glass‐fiber filters. Limnol Oceanogr 38: 1321-1327
673 Corno G, Letelier RM, Abbott MR, Karl DM (2006) Assessing primary production variability in the
674 north pacific subtropical gyre: a comparison of fast repetition rate fluorometry and ^{14}C
675 measurements. J Phycol 42: 51-60
676 Cullen JJ (2001) Primary production methods. In: Steele JH, Turekian KKm Thorpe SA
677 Encyclopedia of Ocean Sciences. Elsevier, Amsterdam, p 2277-2284
678 Davison IR (1991) Environmental effects on algal photosynthesis: temperature. J Phycol 27: 2-8.
679 Dimier C, Corato F, Saviello G, Brunet C (2007) Photophysiological properties of the marine
680 picoeukaryote Picochlorum RCC 237 (Trebouxiophyceae, Chlorophyta). J Phycol
681 43:275-283
682 Dimier C, Brunet C, Geider R, Raven J (2009) Growth and photoregulation dynamics of the
683 picoeukaryote Pelagomonas calceolata in fluctuating light. Limnol Oceanogr 54:823-836
684 Eppley RW, Sharp JH (1975) Photosynthetic measurements in the central North Pacific: the dark
685 loss of carbon in 24 h incubations. Limno Oceanogr 20: 981-987
686 Fujiki T, Hosaka T, Kimoto H, Ishimaru T, Saino T (2008) In situ observation of phytoplankton
687 productivity by an underwater profiling buoy system: use of fast repetition rate fluorometry.
688 Mar Ecol Prog Ser 353: 81-88
689 Giannini MFC, Ciotti M (2016) Parameterization of natural phytoplankton photo‐physiology:
690 Effects of cell size and nutrient concentration. Limnol Oceanogr 61:1495-1512
691 Gong GC, Wen YH, Wang BW, Liu GJ (2003) Seasonal variation of chlorophyll a concentration,

692 primary production and environmental conditions in the subtropical East China Sea. Deep
693 Sea Res II 50: 1219-1236
694 Guo X, Miyazawa Y, Yamagata, T (2006) The Kuroshio onshore intrusion along the shelf break of
695 the East China Sea: the origin of the Tsushima Warm Current. J Phys Oceanogr 36:
696 2205-2231
697 Halsey KH, Jones BM (2015) Phytoplankton strategies for photosynthetic energy allocation. Annu
698 Rev Mar Sci 7: 265-297
699 Halsey KH, Milligan AJ, Behrenfeld MJ (2010) Physiological optimization underlies growth
700 rate-independent chlorophyll-specific gross and net primary production. Photosynth Res 103:
701 125–137
702 Halsey KH, Milligan AJ, Behrenfeld MJ (2011) Linking time-dependent carbon- fixation
703 efficiencies in Dunaliella tertiolecta (Chlorophyceae) to underlying metabolic pathways. J
704 Phycol 47: 66–76
705 Halsey KH, Milligan AJ, Behrenfeld MJ (2014) Contrasting strategies of photosynthetic energy
706 utilization drive lifestyle strategies in ecologically important picoeukaryotes. Metabolites, 4:
707 260-280
708 Hama T, Miyazaki T, Ogawa Y, Iwakuma T, Takahashi M, Otsuki A, Ichimura S (1983)
709 Measurement of photosynthetic production of a marine phytoplankton population using a
710 stable ^{13}C isotope. Mar Biol 73: 31-36
711 Hancke K, Dalsgaard T, Sejr MK, Markager S, Glud, RN (2015) Phytoplankton Productivity in an
712 Arctic Fjord (West Greenland): Estimating Electron Requirements for Carbon Fixation and
713 Oxygen Production. PLOS ONE 10**:** e0133275
714 Hirata T, Aiken J, Hardman-Mountford N, Smyth T, Barlow R (2008) An absorption model to

715 determine phytoplankton size classes from satellite ocean colour. Remote Sens Environ 112:
716 3153-3159
717 Hoppe CJ, Holtz LM, Trimborn S, Rost B (2015) Ocean acidification decreases the light‐use
718 efficiency in an Antarctic diatom under dynamic but not constant light. New Phytol 207:
719 159-171
720 Ichikawa H, Beardsley RC (2002) The current system in the Yellow and East China Seas. J
721 Oceanogr 58: 77-92
722 Jassby AD, Platt T (1976) Mathematical formulation of the relationship between photosynthesis and
723 light for phytoplankton. Limnol Oceanogr 21:540-547
724 Kameda T, Ishizaka J (2005) Size-fractionated primary production estimated by a
725 two-phytoplankton community model applicable to ocean color remote sensing. J Oceanogr
726 61: 663-672
727 Kolber ZS, Prášil O, Falkowski PG (1998) Measurements of variable chlorophyll fluorescence
728 using fast repetition rate techniques: defining methodology and experimental protocols.
729 Biochim Biophys Acta 1367: 88-106
730 Kolber ZS, Falkowski PG (1993) Use of active fluorescence to estimate phytoplankton
731 photosynthesis in situ. Limnol Oceanogr 38:1646-1665
732 Kromkamp JC, Dijkman NA, Peene J, Simis SG, Gons HJ (2008) Estimating phytoplankton
733 primary production in Lake IJsselmeer (The Netherlands) using variable fluorescence
734 (PAM-FRRF) and C-uptake techniques. Eur J Phycol 43: 327-344
735 Lavaud J, Van Gorkom HJ, Etienne AL (2002) Photosystem II electron transfer cycle and
736 chlororespiration in planktonic diatoms. Photosynth Res 74: 51-59
737 Lavaud J, Strzepek RF, Kroth PG. (2007) Photoprotection capacity differs among diatoms: possible

738 consequences on the spatial distribution of diatoms related to fluctuations in the underwater
739 light climate. Limnol Oceanogr 52: 1188-1194
740 Lawrenz E, Silsbe G, Capuzzo E, Ylöstalo P, Forster RM and others (2013) Predicting the Electron
741 Requirement for Carbon Fixation in Seas and Oceans. PLOS ONE 8(3): e58137.
742 doi:10.1371/journal.pone.0058137
743 Liu HC, Shih CY, Gong GC, Ho TY, Shiah FK, Hsieh CH, Chang J (2013) Discrimination between
744 the influences of river discharge and coastal upwelling on summer microphytoplankton
745 phosphorus stress in the East China Sea. Cont Shelf Res 60:104-112
746 Mackey KR, Paytan A, Grossman AR, Bailey S (2008) A photosynthetic strategy for coping in a
747 high‐light, low‐nutrient environment. Limnol Oceanogr 53: 900-913
748 Malone TC (1980) Size-fractionated primary productivity of marine phytoplankton In: Falkowski
749 PG Primary productivity in the sea. Springer, New York, p 301-319
750 Marra JF (2015) Ocean productivity: A personal perspective since the first Liege Colloquium. J
751 Marine Syst 147: 3-8
752 Marra JF, Trees CC, O'reilly JE (2007) Phytoplankton pigment absorption: a strong predictor of
753 primary productivity in the surface ocean. Deep Sea Res I 54: 155-163
754 Mehler AH (1951) Studies on reactions of illuminated chloroplasts. I. Mechanism of the reduction
755 of oxygen and other Hill reagents. Arch Biochem Biophys 33: 65–77
756 Melrose DC, Oviat, CA, O'reilly JE, Berman MS (2006) Comparisons of fast repetition rate
757 fluorescence estimated primary production and ^{14}C uptake by phytoplankton. Mar Ecol Prog
758 Ser 311: 37-46
759 Mino Y, Matsumura S, Lirdwitayaprasit T, Fujiki T, Yanagi T, Saino T (2014) Variations in
760 phytoplankton photo-physiology and productivity in a dynamic eutrophic ecosystem: a fast

761 repetition rate fluorometer-based study. J Plankton Res 36: 398-411
762 Montecino V, Quiroz D (2000) Specific primary production and phytoplankton cell size structure in
763 an upwelling area off the coast of Chile (30 S). Aquat Sci 62**:** 364-380
764 Moore CM, Suggett DJ, Hickman AE, Kim Y-N, Tweddle JF and others. (2006) Phytoplankton
765 photoacclimation and photoadaptation in response to environmental gradients in a shelf sea.
766 Limnol Oceanogr 51:936-949
767 Morimoto A, Takikawa T, Onitsuka G, Watanabe A, Moku M, Yanagi T (2009) Seasonal variation
768 of horizontal material transport through the eastern channel of the Tsushima Straits. J
769 Oceanogr 65: 61-71
770 Murphy, CD, Ni G, Li G, Barnett A, Xu K, Grant-Burt J, Liefer JD, Suggett DJ, Campbell DA
771 (2016), Quantitating active photosystem II reaction center content from fluorescence
772 induction transients. Limnol Oceanogr Methods doi:10.1002/lom3.10142
773 Murtagh F, Legendre P (2014) Ward's hierarchical agglomerative clustering method: Which
774 algorithms implement ward's criterion? J Classif 31:274-295
775 Ning XR, Liu ZL, Cai YM, Fang M, Chai F (1998) Physicobiological oceanographic remote
776 sensing of the East China Sea: Satellite and in situ observations. J Geophys Res 103:
777 21623-21635
778 Oxborough K, Moore CM, Suggett DJ, Lawson T, Chan HG, Geider RJ (2012) Direct estimation of
779 functional PSII reaction center concentration and PSII electron flux on a volume basis: a
780 new approach to the analysis of Fast Repetition Rate fluorometry (FRRf) data. Limnol
781 Oceanogr Methods 10**:** 142-154
782 Parker MS, Armbrust E (2005) Synergistic effects of light, temperature, and nitrogen source on
783 transcription of genes for carbon and nitrogen metabolism in the centric diatom

784 Thalassiosira pseudonana (Bacillariophyceae). J Phycol 41: 1142-1153
785 Pedersen MF, Borum J (1996) Nutrient control of algal growth in estuarine waters. Nutrient
786 limitation and the importance of nitrogen requirements and nitrogen storage among
787 phytoplankton and species of macroalgae. Mar Ecol Prog Ser 142: 261-272
788 Ralph PJ, Wilhelm C, Lavaud J, Jakob T, Petrou K, Kranz SA. (2010) Fluorescence as a tool to
789 understand changes in photosynthetic electron flow regulation. In: Suggett DJ, Prasil O,
790 Borowitzka MA Chlorophyll a Fluorescence in Aquatic Sciences: Methods and Applications.
791 Springer, Netherlands, p 75-89
792 Riegman R, Kuipers BR, Noordeloos AA, Witte HJ (1993) Size-differential control of
793 phytoplankton and the structure of plankton communities. Neth J Sea Res 31:255-265
794 Roberty S, Bailleul B, Berne N, Franck F, Cardol P (2014). PSI Mehler reaction is the main
795 alternative photosynthetic electron pathway in Symbiodinium sp., symbiotic dinoflagellates
796 of cnidarians. New Phytol 204: 81-91
797 Robinson C, Suggett DJ, Cherukuru N, Ralph PJ, Doblin MA (2014) Performance of fast repetition
798 rate fluorometry based estimates of primary productivity in coastal waters. J Mar Syst
799 139:299-310
800 Schuback N, Schallenberg C, Duckham C, Maldonado MT, Tortell PD (2015) Interacting effects of
801 light and iron availability on the coupling of photosynthetic electron transport and
802 CO_2-assimilation in marine phytoplankton. PLOS ONE 10: e0133235
803 Schuback N, Flecken M, Maldonado MT, Tortell PD (2016) Diurnal variation in the coupling of
804 photosynthetic electron transport and carbon fixation in iron-limited phytoplankton in the
805 NE subarctic Pacific. Biogeosciences 13: 1019-1035
806 Schuback N, Hoppe CJ, Tremblay JÉ, Maldonado MT, Tortell PD (2017) Primary productivity and

807 the coupling of photosynthetic electron transport and carbon fixation in the Arctic Ocean.
808 Limnol Oceanogr 62: 898–921. doi:10.1002/lno.10475
809 Silsbe GM, Oxborough K, Suggett DJ, Forster RM and others (2015) Toward autonomous
810 measurements of photosynthetic electron transport rates: An evaluation of active
811 fluorescence ‐ based measurements of photochemistry. Limnol Oceanogr Methods
812 13:138-155
813 Silsbe GM, Behrenfeld MJ, Halsey KH, Milligan AJ, Westberry TK (2016) The CAFE model: A net
814 production model for global ocean phytoplankton. Global Biogeochem Cycles 30: 1756–
815 1777,doi:10.1002/2016GB005521
816 Simis SG, Huot Y, Babin M, Seppälä J, Metsamaa L (2012) Optimization of variable fluorescence
817 measurements of phytoplankton communities with cyanobacteria. Photosynth Res 112:13-30
818 Siswanto E, Ishizaka J, Yokouchi K (2006) Optimal primary production model and parameterization
819 in the eastern East China Sea. J Oceanogr 62: 361-372
820 Suggett DJ, Moore CM, Hickman AE, Geider RJ (2009b) Interpretation of fast repetition rate (FRR)
821 fluorescence: signatures of phytoplankton community structure versus physiological state.
822 Mar Ecol Prog Ser 376:1-19
823 Suggett DJ, Macintyre HL, Kana TM, Geider RJ (2009a) Comparing electron transport with gas
824 exchange: parameterising exchange rates between alternative photosynthetic currencies for
825 eukaryotic phytoplankton. Aquat Microb Ecol 56:147-162
826 Suggett DJ, Maberly SC, Geider RJ (2006a) Gross photosynthesis and lake community metabolism
827 during the spring phytoplankton bloom. Limnol Oceanogr 51: 2064-2076
828 Suggett DJ, Moore CM, Marañón E, Omachi C, Varela RA, Aiken J, Holligan PM (2006b)
829 Photosynthetic electron turnover in the tropical and subtropical Atlantic Ocean. Deep Sea

Res II 53:1573-1592

Suggett DJ, Moore CM, Geider RJ (2010) Estimating aquatic productivity from active fluorescence measurements In: Suggett DJ, Prasil O, Borowitzka MA Chlorophyll a Fluorescence in Aquatic Sciences: Methods and Applications. Springer, Netherlands, p 103-127

Suggett DJ, Macintyre HL, Geider RJ (2004) Evaluation of biophysical and optical determinations of light absorption by photosystem II in phytoplankton. Limnol Oceanogr Methods 2:316-332

Suggett DJ, Warner ME, Smith DJ, Davey P, Hennige S, Baker NR (2008) photosynthesis and production of hydrogen peroxide by symbiodinium (pyrrhophyta) phylotypes with different thermal tolerances. J Phycol 44**:**948-956

Sunda WG, Huntsman SA (1997) Interrelated influence of iron, light and cell size on marine phytoplankton growth. Nature 390:389-392

Suzuki R, Ishimaru T (1990) An improved method for the determination of phytoplankton chlorophyll using N, N-dimethylformamide. J Oceanogr Soc Japan 46:190-194

Thornton DC (2014) Dissolved organic matter (DOM) release by phytoplankton in the contemporary and future ocean. Eur J Phycol 49: 20-46

Tripathy SC, Pavithran S, Sabu P, Naik R, Noronha S, Bhaskar P, Kumar NA (2014) Is primary productivity in the Indian Ocean sector of Southern Ocean affected by pigment packaging effect? Curr Sci 107:1019-1026

Tripathy SC, Ishizaka J, Fujiki T, Shibata T, Okamura K, Hosaka T, Saino T. (2010) Assessment of carbon-and fluorescence-based primary productivity in Ariake Bay, southwestern Japan. Estuar Coast Shelf Sci87:163-173

Uitz J, Claustre H, Morel A, Hooker SB (2006) Vertical distribution of phytoplankton communities

in open ocean: An assessment based on surface chlorophyll. J Geophys Res 111:C08005, doi:10.1029/2005JC003207

Van Heukelem L, Thomas CS (2001) Computer-assisted high-performance liquid chromatography method development with applications to the isolation and analysis of phytoplankton pigments. J Chromatogr A 910: 31-49

Vidussi F, Claustre H, Manca BB, Luchetta A, Marty JC (2001) Phytoplankton pigment distribution in relation to upper thermocline circulation in the eastern Mediterranean Sea during winter. J Geophys Res 106:19939-19956

Wang S, Ishizaka J, Yamaguchi H, Tripathy SC, Hayashi M, Xu Y, Mino Y, Matsuno T, Watanabe Y, Yoo S (2014) Influence of the Changjiang River on the light absorption properties of phytoplankton from the East China Sea. Biogeosciences 11:1759-1773

Wang S, Ishizaka J, Hirawake T, Watanabe Y, Zhu Y, Hayashi M, Yoo S (2015) Remote estimation of phytoplankton size fractions using the spectral shape of light absorption. Opt Express 23**:**10301-10318

Zhu Y, Ishizaka J, Tripathy SC, Wang S, Mino Y, Matsuno T, Suggett DJ (2016) Variation of the photosynthetic electron transfer rate and electron requirement for daily net carbon fixation in Ariake Bay, Japan. J Oceanogr 72:761-776

Figure/table legends

Fig.1 Study area and sampling locations. Main currents during summer period are also shown, Kuroshio Water (KW), Kuroshio Branch Water (KBW), Taiwan Warm Current (TWC), Yellow Sea Cold Water (YSCW), Tsushima Strait Warm Current (TSWC) and Changjiang Diluted Water (CDW) (Ichikawa and Beardsley, 2002). The light grey lines indicate the isobath. The numbers shown besides each station name, represent year of the cruise when the station was sampled. G1'10 contains two sampling points which are G1-1'10 and G1-2'10 at same location.

Fig. 2 Four examples of time series of electron transport rate (ETR_{RCII} ,(mol e^- mol $RCII^{-1}$ s^{-1})) at surface (black circles) and subsurface chlorophyll a maximum (SCM, red circles) with surface instantaneous Photosynthetically Active Radiation (PAR, gray bars). Data of (a) G1-2'10, (b) G1'11, (c) B1'12 and (d) G2'14 were presented. Vertical bars indicate the standard deviations of data included in the upper mixed and SCM layer, respectively.

Fig. 3 (a) Plots of all data of daily ETR (mmol e^- [mgChl-a]$^{-1}$ d^{-1}) versus daily PAR (mol quanta m^{-2} d^{-1}). **(b)** Scatter plots of Chl-a normalised primary productivity (P^B, mg C [mgChl-a]$^{-1}$ d^{-1}) versus daily PAR. **(c)** P^B (mmol C [mgChl-a]$^{-1}$ d^{-1}) versus daily ETR (mmol e^- [mgChl-a]$^{-1}$ d^{-1}). **(d)** Scatter plots of K_C (mol e^- (mol C)$^{-1}$) versus daily PAR (mol quanta m^{-2} d^{-1}) for data divided into upper mixed layer (gray) and other depths (white).Vertical bars represent standard deviations of the P^B and K_C from three replicates for the sampling depth. Type II linear regression was fitted for all data in panel (d).

Fig. 4 (a) Hierarchical cluster analysis (HCA) of stations based on relative contribution physicochemical parameters (sea surface temperature, salinity, NO_3^-+NO_2^- , PO_4^{3-}, mixed layer depth (MLD) and light diffuse attenuation K_d(PAR)). Result of HCA identified two main clusters A and B. **(b)** Scatter plots of daily PAR (mol quanta m^{-2} d^{-1}) and K_C (mol e^- (mol C)$^{-1}$) for two clusters separately. Equations are from Type II linear regressions; red and blue colours in represent different cluster data.

Fig. 5 (a) Boxplot of variability of K_C in each dominant size group (micro-, nano- and pico-dominated). Boxes represent the median, 0.25 and 0.75 quartile, whiskers are the 1.5 interquartile range. Outlier (1.5 times the interquartile range above the upper quartile) is indicated by open circles. Scatter plots of daily PAR (mol quanta m^{-2} d^{-1}) and K_C (mol e^- (mol C)$^{-1}$) for **(b)** 3 size (micro, nano and pico) dominated groups and **(c)** for and for 2 size (micro and nano + pico) dominated groups. Vertical bars represent standard deviations from three replicates. Equations are from Type II linear regressions. Blue, red and green colours in fig. b and c represent different size grouped data.

Fig 6. The biplot of two dimensional NMDS. Coloured labels are sampling points, blue arrows are environmental/community factors.

Table 1 Stations, geographical locations, time of sampling and environmental characteristics during the sampling campaigns.

Table 2 Definitions of photosynthetic parameters used in this text.

Table 3 Mean (± SE, standard error) Chl-a normalised primary productivity (P_B^C, mg C [mgChl-a]$^{-1}$ d^{-1}) and volume-normalised primary productivity (P^C, mgC m^{-3} d^{-1}) measured for the upper mixed versus deep chlorophyll maxima (DCM) water, as well as column integrated PP (PP_{eu}, mgC m^{-2} d^{-1}) of two main study regions.

Table 4 Mean (± SE, standard error) of environmental parameters and phytoplankton size fractions constituting phytoplankton populations and for values of K_C of the upper mixed layer populations within Cluster A and B (see Fig. 4). Welch t-test results are shown comparing the difference between the two clusters. Value in bold indicate significant correlations where $p < 0.05$.

Table 5 Mean (± SE, standard error) of phytoplankton size composition (%) and associated K_C values (mol e$^-$ (mol C)$^{-1}$) for all data binned according to dominance by each of the three size groups (see main text). Welch t-test results are shown comparing the difference between the three size groups. Value in bold indicate significant correlations where $p < 0.01$.

Table 6 Summary of mean value (standard errors) of ETR, P^B and K_C at upper mixed layer of two dominated size classes of phytoplankton. Welch t-test results were presented for examining the significant difference of parameters between two groups. Value in bold indicate significant correlations where $p < 0.01$.

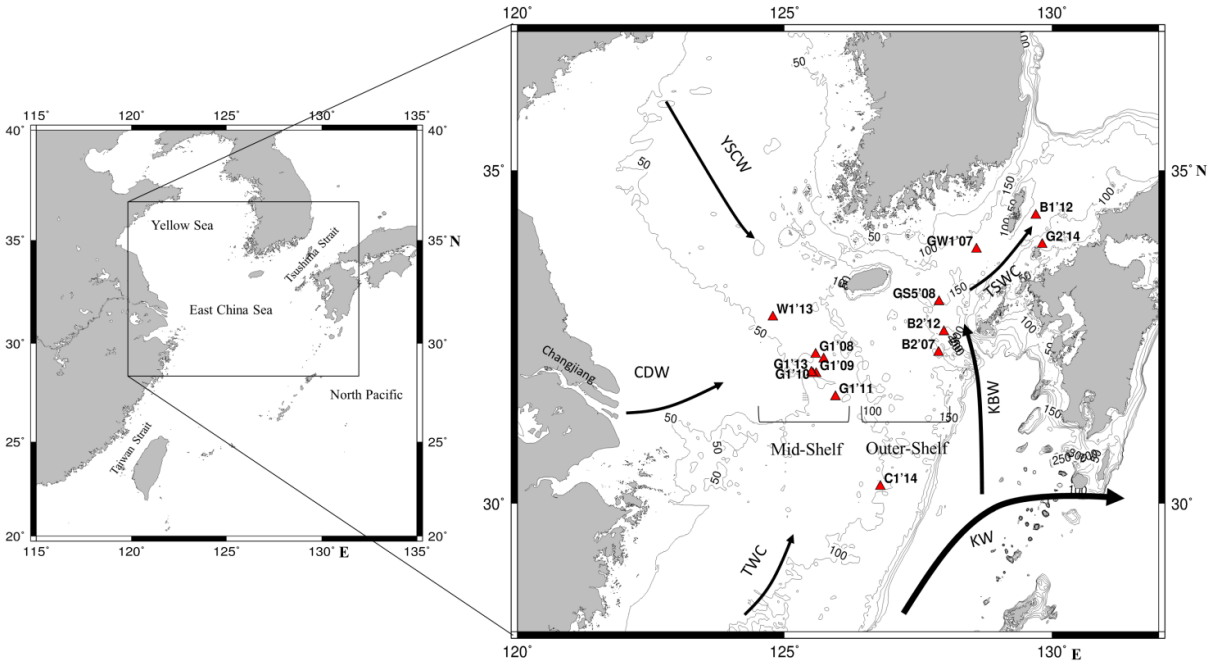
Yellow Sea
East China Sea
North Pacific
Tsushima Strait
Taiwan Strait
YSCW
CDW
TWC
TSWC
KBW
KW
Changjiang
Mid-Shelf
Outer-Shelf
W1'13
G1'08
G1'13
G1'10
G1'09
G1'11
GS5'08
B2'12
B2'07
GW1'07
B1'12
G2'14
C1'14

Fig.1

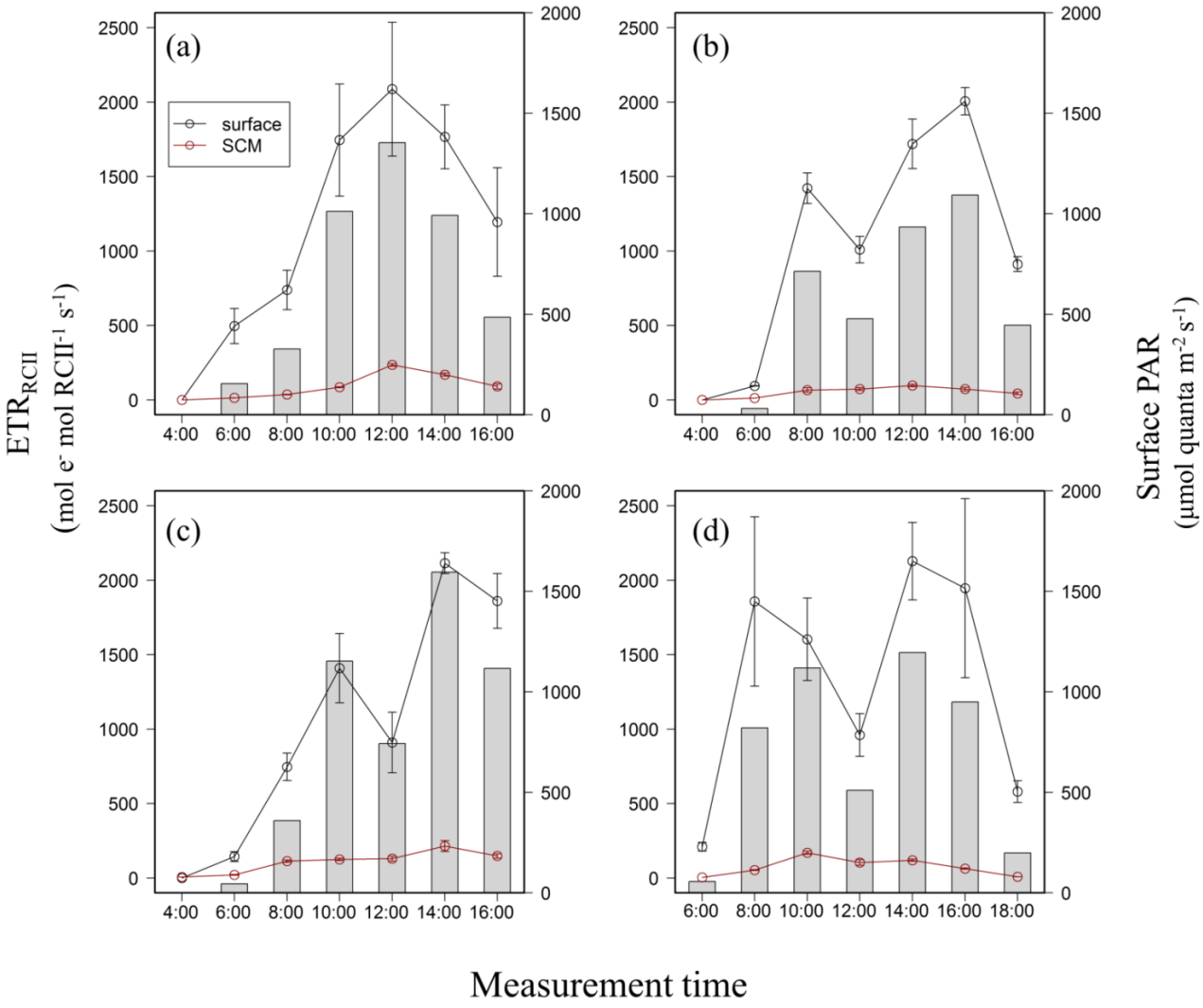

952

953 **Fig.2**

954

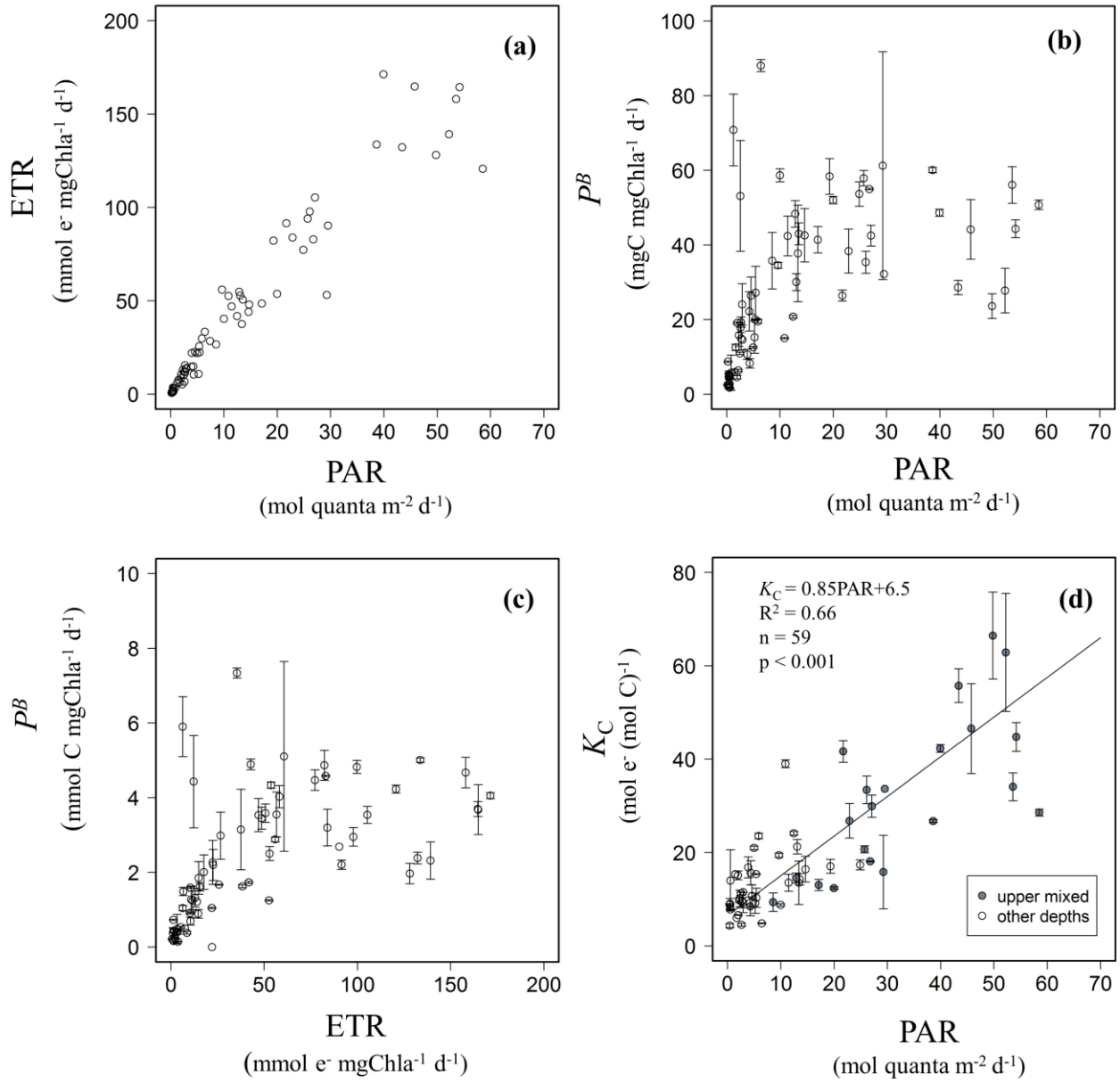
(a)
ETR
(mmol e- mgChla-1 d-1)
PAR
(mol quanta m-2 d-1)
(b)
PB
(mgC mgChla-1 d-1)
PAR
(mol quanta m-2 d-1)
(c)
PB
(mmol C mgChla-1 d-1)
ETR
(mmol e- mgChla-1 d-1)
(d)
KC = 0.85PAR+6.5
R2 = 0.66
n = 59
p < 0.001
KC
(mol e- (mol C)-1)
upper mixed
other depths
PAR
(mol quanta m-2 d-1)

Fig.3

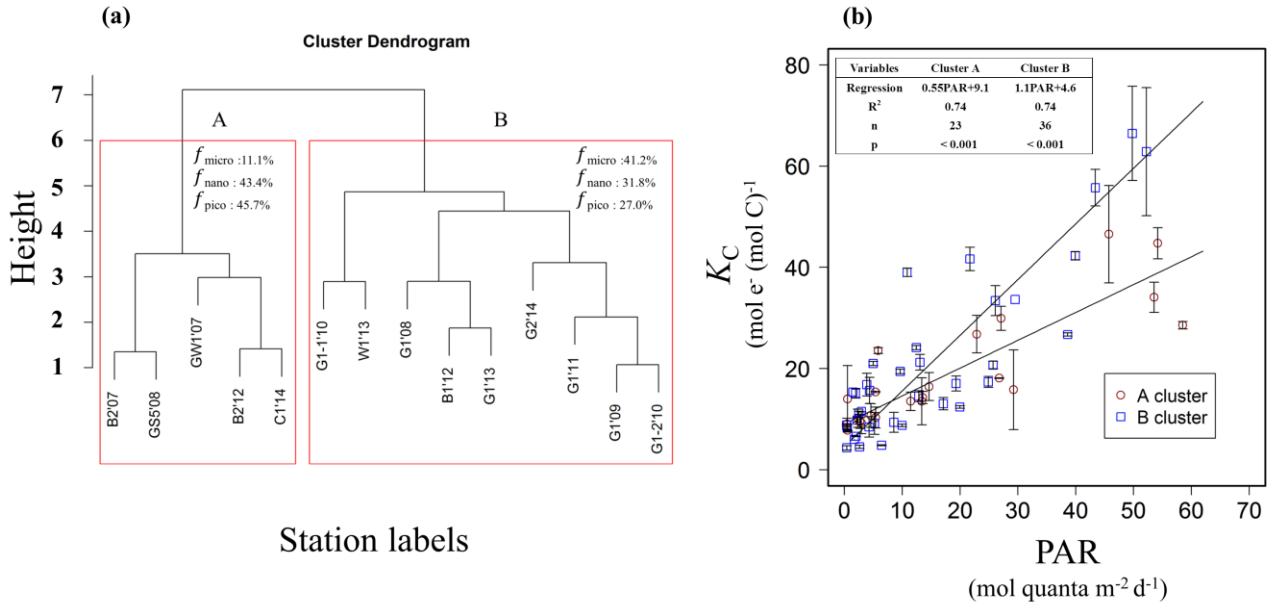
(a)
Cluster Dendrogram
Height
A
B
f_{micro} :11.1%
f_{nano} : 43.4%
f_{pico} : 45.7%
f_{micro} :41.2%
f_{nano} : 31.8%
f_{pico} : 27.0%
B2'07
GS5'08
GW1'07
B2'12
C1'14
G1-1'10
W1'13
G1'08
B1'12
G1'13
G2'14
G1'11
G1'09
G1-2'10
Station labels
(b)
Variables
Cluster A
Cluster B
Regression
0.55PAR+9.1
1.1PAR+4.6
R^2
0.74
0.74
n
23
36
p
< 0.001
< 0.001
A cluster
B cluster
K_C
(mol e$^-$ (mol C)$^{-1}$
PAR
(mol quanta m^{-2} d^{-1})

Fig.4

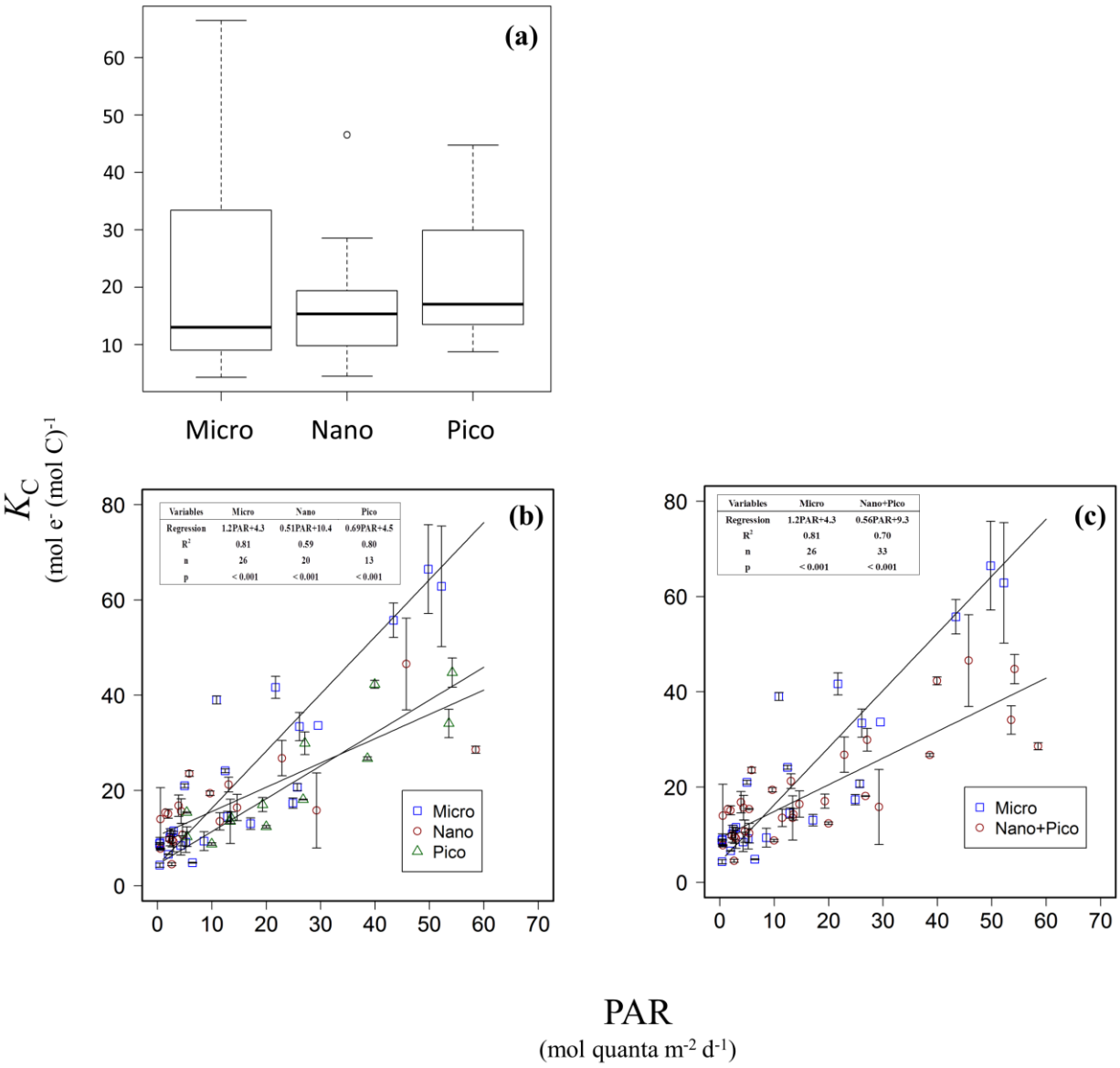
(a)
Micro
Nano
Pico
(b)
Variables Micro Nano Pico
Regression 1.2PAR+4.3 0.51PAR+10.4 0.69PAR+4.5
R² 0.81 0.59 0.80
n 26 20 13
p < 0.001 < 0.001 < 0.001
Micro
Nano
Pico
(c)
Variables Micro Nano+Pico
Regression 1.2PAR+4.3 0.56PAR+9.3
R² 0.81 0.70
n 26 33
p < 0.001 < 0.001
Micro
Nano+Pico
K_C
(mol e⁻ (mol C)⁻¹
PAR
(mol quanta m⁻² d⁻¹)

Fig.5

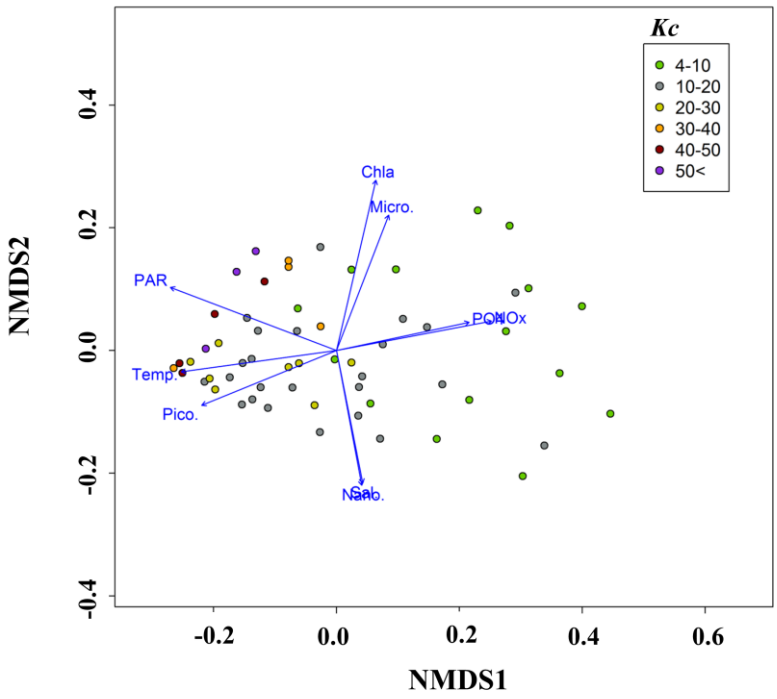
Kc
4-10
10-20
20-30
30-40
40-50
50<
Chla
Micro.
PAR
PCHOx
Temp.
Pico.
Nano.
NMDS1
NMDS2
0.6
0.4
0.2
0.0
-0.2
-0.4

967

968 **Fig.6**

969 **Table 1**

No.	Date	Station	Location	Daily PAR (E_0^+, mol quanta m^{-2} d^{-1})	Depth of upper mixed layer (m)	Depth of deep Chl-a maxima (m)	Z_{eu} (1% surface PAR, m)	FRRf Observation periods
1	23 July, 2007	GW1'07	33.84 N, 128.59 E	60.2	14	34	60	6:00 – 10:00
2	26 July, 2007	B2'07	32.3 N, 127.88 E	59.5	10	65	85	6:00 – 18:00
3	25 July, 2008	GS5'08	33.06 N, 127.89 E	50.4	13	42	65	6:00 – 10:00
4	11 Aug., 2008	G1'08	32.27 N, 125.58 E	44.4	10	NA[b]	22	6:00 – 18:00
5	20 July, 2009	G1'09	32.27 N, 125.59 E	28.6	4	13	26	4:00 – 16:00
6	19 July, 2010	G1-1'10	31.98 N, 125.53 E	58.0	6	20	35	4:00 – 16:00
7	23 July, 2010	G1-2'10	32.2 N, 125.73 E	48.2	4	20	35	4:00 – 16:00
8	21 July, 2011	G1'11	31.63 N, 125.95 E	42.9	2	30	35	4:00 – 16:00
9[a]	22 July, 2012	B1'12	34.34 N, 129.7 E	51.2	8	43	47	4:00 – 16:00
10[a]	25 July, 2012	B2'12	32.61 N, 127.98 E	43.3	5	57	70	4:00 – 16:00
11	23 July, 2013	G1'13	32.0N, 125.5E	32.8	10	30	32	4:00 – 10:00
12	26 July, 2013	W1'13	32.83 N, 124.78 E	19.1	4	10	21	4:00 – 18:00
13	21 July, 2014	C1'14	30.26 N, 126.79 E	65.0	5	42	55	6:00 – 18:00
14	26 July, 2014	G2'14	33.91 N, 129.82 E	55.3	2	40	50	6:00 – 18:00

[a] no ^{13}C data

[b] maxima Chl-a was within upper mixed layer

970
971
972
973
974
975
976
977

Table 2

Parameter	Definition
PAR	Instantaneous irradiance (µmol quanta m^{-2} s^{-1})
Daily PAR	Daily integrated irradiance (mol quanta m^{-2} d^{-1})
F_o	Minimum fluorescence yield in dark chamber (arbitrary units: a.u.)
F_m	Maximum fluorescence yield in dark chamber (a.u.)
F_v/F_m	Potential photochemical efficiency of open reaction centers [=(F_m - F_o)/ F_m] (dimensionless)
F'	Steady-state fluorescence yields in light chamber (a.u.)
F_m'	Maximum fluorescence yield in light chamber (a.u.)
F_q'/F_m'	Photochemical efficiency of PSII under actinic light
q_p (F_q'/F_v')	Photochemical quenching coefficient, as the difference in the apparent PSII photochemical efficiency between FRRf light and dark chamber quasi-simultaneously,= $[\frac{(F_m' - F')/F_m'^{\ \text{light chamber}}}{(F_m - F_o)/F_m^{\ \text{dark chamber}}}]$[a], (dimensionless)
n_{PSII}	Photosynthetic unit size of PSII (mol RCII (mol Chla)$^{-1}$)
σ_{PSII}	Effective absorption cross section of PSII in dark chamber (Å^2 quanta^{-1})
σ_{PSII}^{470}	Effective absorption cross section of PSII in dark chamber (Å^2 quanta^{-1})
σ_{PSII}^{abs}	Spectral corrected effective absorption cross section of PSII (Å^2 quanta^{-1})
ETR_{RCII}	electron transport rate per RCII (mol e^- mol RCII^{-1} s^{-1})
Daily ETR	Chla specific daily electron transport rate through PSII (mmol e^- (mg Chl-a)$^{-1}$ d^{-1})
K_C	Electron requirement for carbon fixation (mol e^- (mol C)$^{-1}$)

[a.] Suggett et al., 2006a,b

Table 3

Region	Layer	P_B^C (mgC mg Chl-a^{-1} d^{-1})	P^C (mgC m^{-3} d^{-1})	$^{a}PP_{eu}$ (mgC m^{-2} d^{-1})
ECS mid-shelf n=7	upper mixed layer	41.5 (4.6)	51.5 (7.2)	853 (97)
	DCM Layer	19.4 (8.2)	31.0 (8.5)	
ECS outer-shelf & TS n=5	upper mixed layer	43.9 (5.3)	5.4 (0.5)	451 (51)
	DCM Layer	16.2 (2.4)	10.1 (2.1)	

$^{a}PP_{eu}$ refers to $P^C(z)$ integrated from surface to Z_{eu}

Table 4

Cluster	physical and biochemical parameters									
	Temp. (℃)	Sal.	NO_x^- (μM)	PO_4^{3-} (μM)	N/P	Chla (mg m^{-3})	Micro (%)	Nano (%)	Pico (%)	*K*c (mol e$^-$ (mol C)$^{-1}$)
A (n=9)	26.9 (0.6)	33.3 (0.3)	0.02 (0.01)	0.01 (0.01)	2.3 (0.9)	0.13 (0.02)	11.1 (3.6)	43.4 (5.6)	45.7 (7.5)	28.7 （1.6）
B (n=15)	26.5 (0.3)	30.5 (0.4)	0.45 (0.15)	0.08 (0.02)	13.9 (7.1)	1.16 (0.25)	41.2 (6.3)	31.8 (3.0)	27.0 (4.7)	34.1 （4.2）
t test	p = 0.5	p = **0.001**	p = 0.07	p= **0.02**	p = 0.3	p= **0.02**	p = **0.007**	p = 0.1	p = 0.06	p = 0.7

Table 5

Dominated groups	Size composition (%)			
	Micro%	Nano%	Pico%	*K*c
Micro- (n=26)	56.4 (2.6)	28.9 (1.8)	14.6 (2.2)	21.8 (3.5)
Nano- (n=20)	23.2 (3.1)	58.5 (2.4)	18.4 (3.1)	16.7 (2.1)
Pico- (n=13)	11.0 (1.3)	35.1 (1.0)	53.8 (2.1)	22.1 (3.2)
t test	p < **0.001**	p < **0.001**	p < **0.001**	p = 0.6

Table 6

Dominated groups	*ETR* (mmol e^- (mg Chl-a)$^{-1}$ d^{-1})	P_B^C *(* mgC mg Chl-a^{-1} d^{-1}*)*	K_C (mol e^- (mol C)$^{-1}$)
Micro (n=11)	91. (10)	35.2 (3.0)	35.0 (5.7)
Nano +Pico (n=13)	109 (10)	46.8 (2.1)	29.2 (2.6)
t-test	p = 0.3	p = **0.01**	p = 0.4

Literature Cited

Ichikawa H, Beardsley RC (2002) The current system in the Yellow and East China Seas. J Oceanogr 58: 77-92

Suggett DJ, Maberly SC, Geider RJ (2006a) Gross photosynthesis and lake community metabolism during the spring phytoplankton bloom. Limnol Oceanogr 51: 2064-2076

Suggett DJ, Moore CM, Marañón E, Omachi C, Varela RA, Aiken J, Holligan PM (2006b) Photosynthetic electron turnover in the tropical and subtropical Atlantic Ocean. Deep Sea Res II 53:1573-1592

Supplementary Material

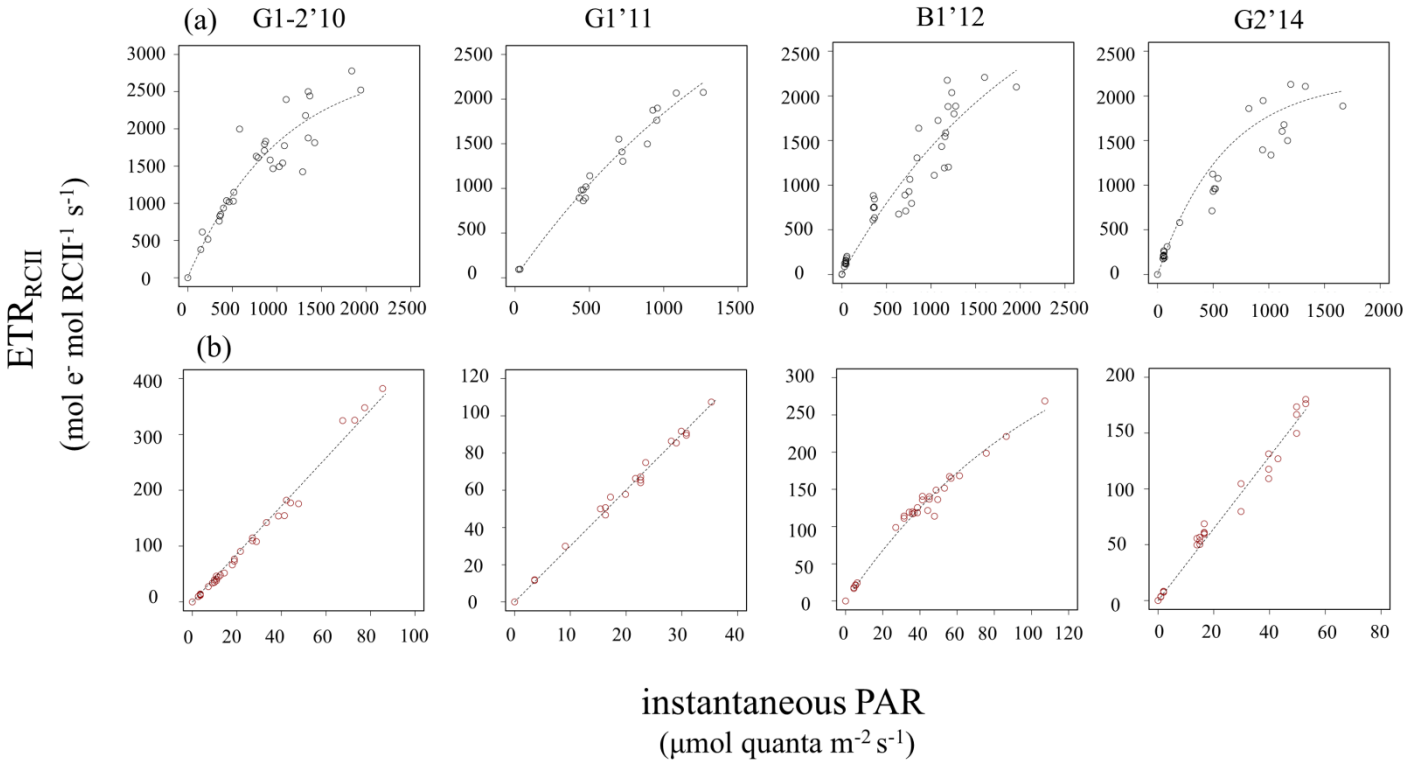

Fig. S1 Examples of the relationship between PAR (µmol quanta m^{-2} s^{-1}) and ETR_{RCII} (mol e^- mol $RCII^{-1}$ s^{-1}) for phytoplankton populations at 4 stations from within the (a) samples for the upper mixed layer data which exposed to light saturating conditions, the relationship between ETR_{RCII} and PAR was described by exponential fits and (b) data from SCM layers where light intensities were not high enough to cause ETR_{RCII} saturation, simple linear least-square regression fitting was employed (except B1'12). Dashed lines are the exponential or linear fittings.

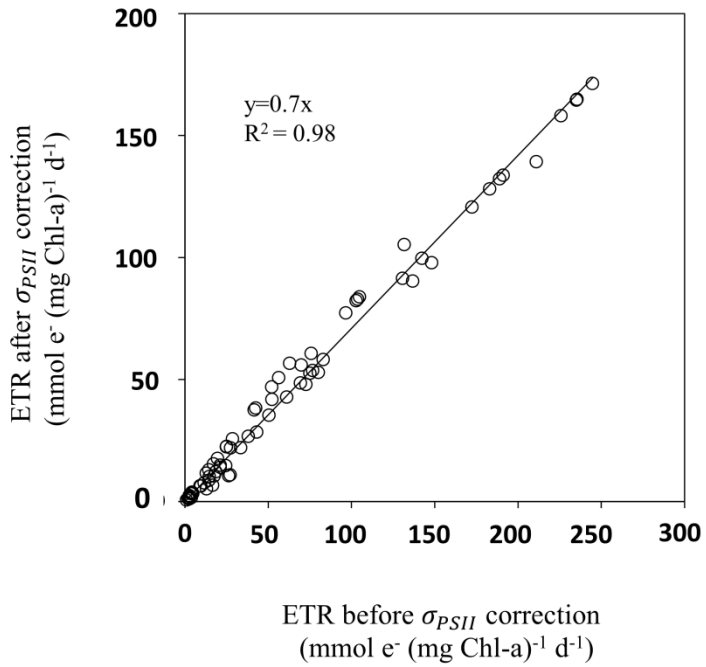

Fig. S2 Plot of ETRs (mmol e^- (mg Chl-a)$^{-1}$ d^{-1}) before and after σ_{PSII} spectra correction.

Table S1 Spearman correlation coefficients for correlations between daily K_C and environmental variables.Temp. = temperature, Sal. = salinity, $a_{ph}^* = a_{ph}^*(440)$, Micro, Nano and Pico represents fraction of micro-, nano- and pico- phytoplankton, respectively.

	PAR	Temp.	Sal.	Chla	NO_3^-+NO_2^-	PO_4^{3-}	DSi	a_{ph}^*	micro	nano	pico
K_C	.798**	.477**	-.165	-.270*	-.512**	-.393**	-.177	.313*	-.344*	-.212	.688**
	n=59	n=59	n=59	n=59	n=59	n=59	n=59	n=46	n=59	n=59	n=59

** indicates significance of the correlation at the 0.01 significant level

* indicates significance of the correlation at the 0.05 significant level

Table S2 Influence of various environmental and biological variable on *K*c, estimated by multiply linear regression analysis. Temp. = temperature, Sal. = salinity, $a_{ph}^* = a_{ph}^*(440)$, N = NO_x^-, P - PO_4^{3-}, Si = DSi. Micro, Nano and Pico represents fraction of micro-, nano- and pico- phytoplankton, respectively.

No. of predictor variables	Variables	R^2
1	PAR	0.662
2	PAR, Chla	0.675
3	PAR, Chla, Temp.	0.683
4	PAR, Chla, Temp. Sal.	0.685
5	PAR, Chla, Temp. Sal. a_{ph}^*	0.685
6	PAR, Chla, Temp. Sal. a_{ph}^*, N	0.700
7	PAR, Chla, Temp. Sal. a_{ph}^*, N, P	0.704
8	PAR, Chla, Temp. Sal. a_{ph}^*, N, P, Si	0.707
9	PAR, Chla, Temp. Sal. a_{ph}^*, N, P, Si, Micro	0.723
10	PAR, Chla, Temp. Sal. a_{ph}^*, N, P, Si, Micro, Nano	0.779
11	PAR, Chla, Temp. Sal. a_{ph}^*, N, P, Si, Micro, Nano, Pico	0.792

Table S3 Mean (standard deviation) of relative $1/n_{PSII}$ with time of day at surface of each cruise. Welch t-test results are shown comparing the difference between the time series mean value.

Station	Relative $1/n_{PSII}$	p
GW1'07	0.88(0.07)	0.08
B2'07	0.86 (0.15)	0.06
GS5'08	0.96 (0.11).	0.10
G1'08	0.95 (0.13)	0.01
G1'09	0.93 (0.1)	0.01
G1-1'10	0.91 (0.06)	0.06
G1-2'10	0.85 (0.13)	0.02
G1'11	0.98 (0.33)	0.01
G1'13	0.71 (0.06)	0.02
W1'13	0.81 (0.11)	0.05
C1'14	0.82 (0.17)	0.11
G2'14	0.83 (0.08)	0.13